10-6-2022

Evidence for the ~ 1.4 Ga Picuris orogeny in the central Colorado Front Range

Asha A. Mahatma

Yvette D. Kuiper

christopher S. Holm-Denoma

Precambrian Research 382 (2022) 106878

Contents lists available at ScienceDirect

Precambrian Research

journal homepage: www.elsevier.com/locate/precamres

Evidence for the ∼ 1.4 Ga Picuris orogeny in the central Colorado Front Range

Asha A. Mahatma [a], Yvette D. Kuiper [a,*], Christopher S. Holm-Denoma [b]

[a] Department of Geology and Geological Engineering, Colorado School of Mines, 1516 Illinois Street, Golden, CO 80401, USA
[b] U.S. Geological Survey, Denver Federal Center, W 6th Ave Kipling St., Denver, CO 80225, USA

ARTICLE INFO

Keywords:
Picuris orogeny
Yavapai
Mazatzal
U–Pb geochronology
Monazite
Detrital zircon

ABSTRACT

We present the first evidence for sedimentation and new evidence for penetrative deformation and metamorphism in the central Colorado Front Range associated with the ∼ 1.48–1.35 Ga Picuris orogeny. This orogeny has recently been recognized in New Mexico, Arizona and southern Colorado and may be part of a larger active accretionary margin that includes the ∼ 1.51–1.46 Ga Pinware and Baraboo events, in eastern Canada and central US respectively, that preceded the amalgamation of the Rodinian supercontinent. We demonstrate that in addition to ∼ 1.4 Ga reactivation of northeast-trending Paleoproterozoic shear zones, regional folding occurred in an area south of Mt. Evans, away from these shear zones.

Detrital zircon from one quartzite yielded U–Pb laser ablation inductively coupled mass spectrometry (LA-ICPMS) major age populations of ∼ 1.81–1.61 Ga and ∼ 1.49–1.38 Ga, and minor ones of ∼ 1.90 Ga and ∼ 1.56 Ga. The Paleoproterozoic and ∼ 1.49–1.38 Ga populations have numerous local and regional sources. The ∼ 1.56 Ga age population may represent a minor exotic population as recognized in Defiance, Arizona the Yankee Joe and Blackjack Formations in Arizona, the Four Peaks area in Arizona, and the Tusas and Picuris Mountains in New Mexico. Alternatively it may be a result of mixing between zircon age domains reflecting the older and younger populations, or Pb loss from 1.81 to 1.61 Ga zircon.

In-situ LA-ICPMS U–Pb analysis on monazite from four biotite schist samples yielded ∼ 1.74 Ga and ∼ 1.42 Ga age populations, and separate populations that show ∼ 1.68–1.47 Ga and ∼ 1.39–1.33 Ga age spreads. The ∼ 1.74 Ga and ∼ 1.68–1.47 Ga populations may be detrital or metamorphic. Monazite ages between ∼ 1.6 Ga and ∼ 1.5 Ga may be due to the mixing of age domains or Pb loss, because metamorphism during that time has not been recognized in Laurentia. The ∼ 1.42 Ga and ∼ 1.39–1.33 Ga populations are most likely metamorphic and consistent with the age of the ∼ 1.48–1.35 Ga Picuris orogeny. The evidence for ∼ 1.4 Ga sedimentation, and especially regional folding and metamorphism in the central Colorado Front Range indicate that the impact and extent of the Picuris orogeny in the southwestern U.S. are larger than previously thought.

1. Introduction

Proterozoic rocks of the central Front Range, Colorado (Fig. 1), record evidence for multiple Proterozoic orogenic events. The earliest were the Paleoproterozoic Yavapai (∼1.75–1.68 Ga) and Mazatzal (∼1.65–1.60 Ga) orogenies, both of which involved the accretion of juvenile crust to Laurentia (e.g., Karlstrom and Bowring 1988; Holland et al., 2020) and may have been a continuous period of deformation (Jones and Connelly, 2006; Mahan et al., 2013). These were followed by the Mesoproterozoic Picuris orogeny, which was first recognized and defined in northern New Mexico (Daniel et al., 2013b), and part of the larger ∼ 1.50–1.35 Ga Pinware–Baraboo–Picuris orogen that extends across North America into Quebec and Labrador, Canada (Fig. 1; Daniel et al., 2022). The extent and the nature of this convergent event in Colorado are largely unknown. In Colorado, ∼1.4 Ga granitoids have historically been interpreted as anorogenic (Anderson, 1983; Bickford et al., 1986; Karlstrom and Bowring, 1988; Goodge and Vervoort, 2006; Whitmeyer and Karlstrom, 2007), but based on deformation of these plutons, some have been interpreted as *syn*-tectonic (Nyman et al., 1994; Selverstone et al., 2000; Gonzales and Van Schmus, 2007; Jones et al., 2010a; Aronoff, 2016). Otherwise, in Colorado, the ∼ 1.4 Ga deformation has been primarily recognized as reactivation along

* Corresponding author.
E-mail address: ykuiper@mines.edu (Y.D. Kuiper).

https://doi.org/10.1016/j.precamres.2022.106878
Received 13 May 2022; Received in revised form 4 October 2022; Accepted 6 October 2022
Available online 21 October 2022

Paleoproterozoic shear zones (Selverstone et al., 2000; Shaw et al., 2001; McCoy et al., 2005, Shaw and Allen, 2007; Allen and Shaw, 2011; Lytle, 2016), while ~ 1.4 Ga penetrative deformation in Paleoproterozoic rocks has only been recognized in the Wet Mountains (Fig. 1; Jones et al., 2010b). Sims and Stein (2003) named the reactivation along shear zones in the Colorado Front Range the 'Berthoud Orogeny'. Some of the folding adjacent to the Idaho Springs–Ralston Shear Zone (Fig. 1) was also ~ 1.4 Ga, but may have been related to the shear movement (Lytle, 2016). In this contribution, we present new structural, petrographic and U–Pb laser ablation inductively coupled mass spectrometry (LA-ICPMS) monazite data, demonstrating evidence for Mesoproterozoic folding in the central Colorado Front Range (Fig. 1), >10 km away from localized shear zones and from Phanerozoic overprinting structures. We also present new U–Pb detrital zircon LA-ICPMS results for a quartzite, showing the first evidence for a Mesoproterozoic quartzite in Colorado. We combined structural and geochronological data from Colorado, New

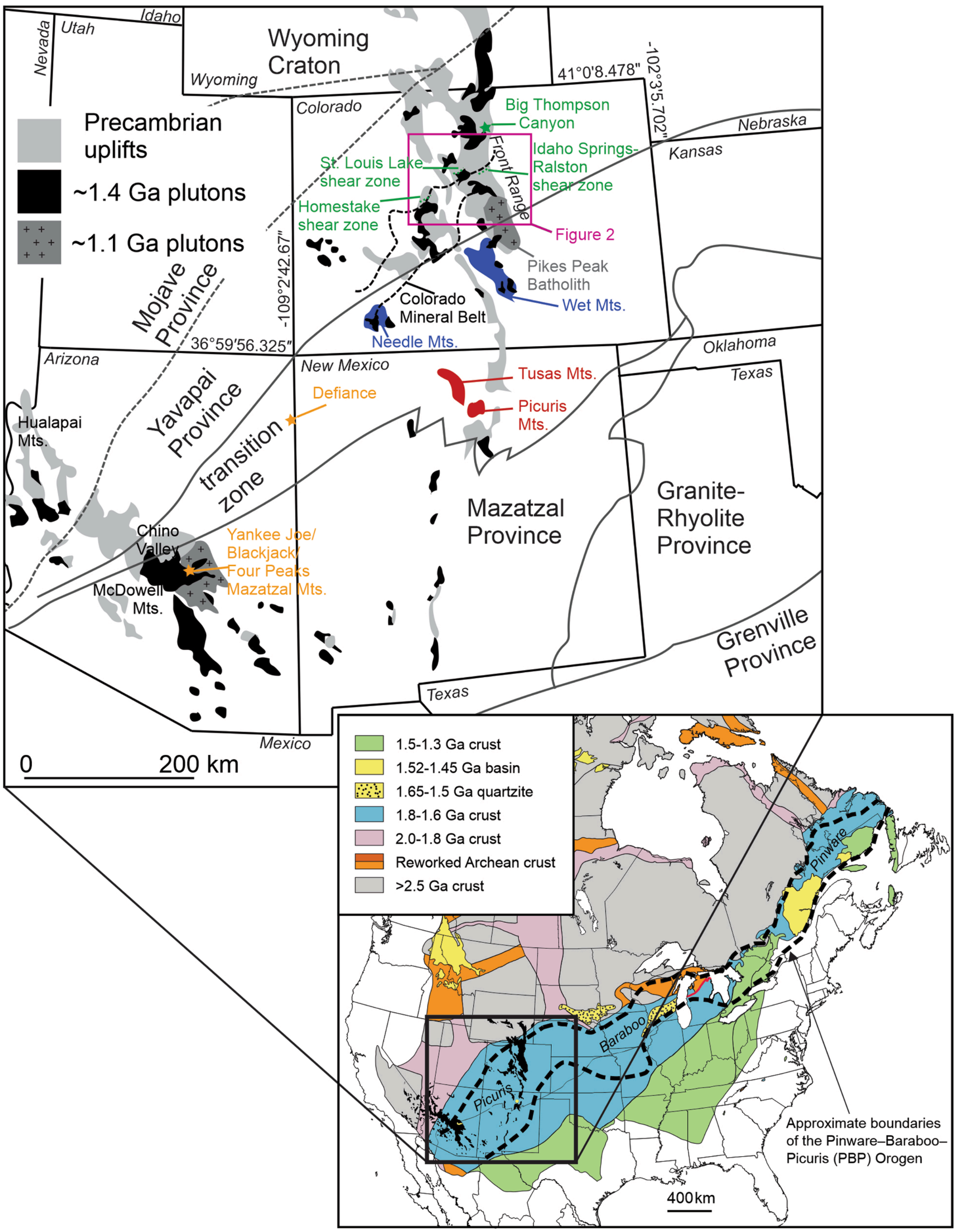

Fig. 1. Simplified map of the southwestern United States showing Proterozoic exposures. Modified after Jones et al. (2010b; cf. Condie, 1986; Bennett and DePaolo, 1987; Karlstrom and Bowring. 1988; Wooden et al., 1988; Wooden and DeWitt, 1991). Inset figure shows setting within North American craton. (modified after Daniel et al., 2022).

Mexico, and Arizona to establish the regional timing of Early Mesoproterozoic sedimentary basins, and the impact, extent and timing of deformation associated with the Pinware–Baraboo–Picuris orogeny.

2. Geologic background

Paleoproterozoic amphibolite-facies metasedimentary and metaigneous rocks of the Colorado Front Range are generally interpreted as juvenile arc terranes and associated basins (e.g. Gable, 2000; Widmann et al., 2000; Kellogg et al., 2008). These terranes amalgamated and accreted to the Archean Wyoming craton, a portion of the Laurentian margin, between ~ 1.8 Ga and ~ 1.6 Ga (Wilson, 1939; Condie, 1982; Karlstrom and Bowring, 1988; Bowring and Karlstrom, 1990; Whitmeyer and Karlstrom, 2007). The addition of these terranes may have been accompanied by a continuous period of deformation, but are generally separated between the Yavapai and Mazatzal orogenies (Jones and Connelly, 2006; Mahan et al., 2013). The ~ 1.72–1.68 Ga Yavapai orogeny was caused by the accretion of ~ 1.78 Ga to ~ 1.72 Ga juvenile arcs of the Yavapai province to the southern margin of Laurentia (Whitmeyer and Karlstrom, 2007). The Yavapai province now exists between Arizona and Michigan (Fig. 1; Holm et al., 2007; Whitmeyer and Karlstrom, 2007). Most of the Proterozoic basement rocks of Colorado are considered to be part of the Yavapai province. This basement was intruded by ~ 1.77–1.67 Ga calc-alkaline plutons (Anderson and Cullers, 1999).

The ~ 1.65–1.60 Ga Mazatzal orogeny has been interpreted as the accretion of ~ 1.68–1.66 Ga crust of the Mazatzal province to Laurentia (Karlstrom and Bowring, 1988). This crust generally formed in a continental margin setting composed of a collage of volcanic arcs and back-arc basins (Whitmeyer and Karlstrom, 2007). The Mazatzal province probably includes older Paleoproterozoic crustal material (Holland et al., 2020). Evidence for the Mazatzal province exists between Arizona in the USA and Labrador in Canada (Fig. 1; Wilson, 1939; Condie, 1982; Karlstrom and Bowring, 1988; Bowring and Karlstrom, 1990; Whitmeyer and Karlstrom, 2007). Deformation in the Mazatzal Mountains of Arizona has now been documented at ~ 1.47–1.43 Ga (Doe et al., 2012; Doe and Daniel, 2019), the general age of the Picuris orogeny, making the name 'Mazatzal orogeny' for the ~ 1.65–1.60 Ga deformation and metamorphism recognized elsewhere controversial (Doe and Daniel, 2019). Between ~ 1.60 Ga and ~ 1.48 Ga Laurentia was tectonically quiescent (Whitmeyer and Karlstrom, 2007; Doe et al., 2012; Aronoff, 2016).

At ~ 1.4 Ga, granitoids were emplaced in a broad belt spanning from the southwestern United States through eastern Canada and into Baltica (Fig. 1; Windley, 1993; Karlstrom and Humphreys, 1998; du Bray et al., 2018). These granitoids may be divided into two temporally dictinct pulses at ~ 1.49–1.41 Ga and ~ 1.41–1.34 Ga (Whitmeyer and Karlstrom, 2007). The granitoids are predominantly ferroan (formerly A-type) granites (e.g. Frost and Frost, 2011; du Bray et al., 2018) and many were historically interpreted as having been emplaced anorogenically (Anderson, 1983; Bickford et al., 1986; Karlstrom and Bowring, 1988; Goodge and Vervoort, 2006; Whitmeyer and Karlstrom, 2007). However, episodes of significant convergent deformation and regional metamorphism are now recognized in parts of New Mexico, Arizona and Colorado at these times of pluton emplacement, and many ~ 1.4 Ga intrusive rocks are now recognized to show tectonic foliation (Grambling and Codding, 1982; Nyman et al., 1994; Gonzales et al., 1996; Selverstone et al., 2000; McCoy, 2001; Daniel and Pyle, 2006; Gonzales and Van Schmus, 2007; Jones et al., 2010a, 2011; Shah and Bell, 2012; Doe et al., 2013; Daniel et al., 2013b; Mahan et al., 2013; Mako et al., 2015; Aronoff, 2016; Lytle, 2016; Doe and Daniel, 2019). This suggests that they are not anorogenic, but emplaced along and inboard of an active plate margin to the southeast (cf. Fig. 1; Daniel et al., 2022).

The Picuris orogeny resulted from ~ 1.5–1.4 Ga convergence along Laurentia's southern margin (Daniel and Pyle, 2006; Aronoff, 2016; Daniel et al., 2022). In northeastern North America, the ~ 1.51–1.46 Ga Pinware orogeny (Fig. 1) involved convergence and subduction within the proto-Grenville province of Labrador and eastern Quebec (Tucker and Gower, 1994; Gower and Krogh, 2002; Daniel et al., 2022). Similarly, ~1.49–1.47 Ga muscovite $^{40}Ar/^{39}Ar$ ages and syntectonic (?) plutons in that same age range support the midcontinent Baraboo orogeny in Wisconsin and beyond (Fig. 1; Medaris et al. (2021)). The ~ 1.48–1.35 Ga Picuris orogeny in northern New Mexico involved convergence and possible collision of juvenile crust with the southern margin of Laurentia (Aronoff, 2016), which was accompanied by shortening and thickening of Paleo- and Mesoproterozoic rocks (Daniel and Pyle, 2006; Daniel et al., 2013b; Aronoff, 2016). The Picuris orogeny is also recognized in parts of northern New Mexico, central Arizona, and Colorado (e.g. Daniel et al., 2022). Mesoproterozoic (~1.45 Ga) sedimentary basins in New Mexico and Arizona (Jones et al., 2011; Doe et al., 2012, 2013; Daniel et al., 2013a,b; Mako, 2014) were deposited prior to, or at the onset of the Picuris orogeny.

The ~ 1.1 Ga Pikes Peak batholith (Figs. 1, 2; Smith et al., 1999; Guitreau et al., 2016) was coeval with the ~ 1.2–1.0 Ga Grenville orogeny along the southeastern margin of Laurentia (e.g. Whitmeyer and Karlstrom, 2007), but no significant deformation occurred as a result of the Grenville orogeny in Colorado. Proterozoic structures in Colorado are overprinted by localized faults formed during the Pennsylvanian-Permian Ancestral Rocky Mountains (Kluth and Coney, 1981; Ye et al., 1996) and the Late Cretaceous–Eocene Laramide orogeny (e.g., English et al., 2003; Kellogg et al., 2008). Paleogene mineralization associated with the Laramide orogeny was concentrated within the Colorado Mineral Belt (Fig. 1) and may have been partially controlled by reactivation of Proterozoic structures, such as shear zones (Tweto and Sims, 1963; Caine et al., 2010; Chapin, 2012). The latest Oligocene deformation is localized extension associated with the northern reach of the Rio Grande Rift, which trends northward from Socorro, New Mexico to Leadville, Colorado (Olsen et al., 1987; Chapin and Cather, 1994; Caine and Minor, 2009; Minor et al., 2013).

3. Field results

Field mapping and sampling were carried out over a three-month period during the summer of 2017 in the southern half of the Mt. Evans 7.5-minute quadrangle as part of a U.S. Geological Survey EdMap program. The full quadrangle will be published at a 1:24,000 scale through the Colorado Geological Survey (Powell et al., 2022). The area (Figs. 2, 3) is mainly composed of Paleo- or Mesoproterozoic metasedimentary and metaigneous rocks, and intrusive granitoid rocks that are most likely Mesoproterozoic (Bryant et al., 1981; Aleinikoff et al., 1993; du Bray et al., 2018). Metamorphic rock types in this area include mafic to felsic gneiss, quartzite, calc-silicate gneiss, amphibolite, and biotite schist and gneiss. The presence of local sillimanite and migmatite in the biotite schist and gneiss indicate that peak metamorphism occurred under upper amphibolite facies conditions. The quartzite used for U–Pb detrital zircon LA-ICPMS analysis in this study occurs in a ~ 200 × 150 m exposure that also contains calc-silicate gneiss and minor amphibolite. The contact between quartzite and calcsilicate/amphibolite is transitional, and the entire package is within biotite schist. On the north side, the calc-silicate gneiss is in contact with Mesoproterozoic granite. The metasedimentary rocks are deformed and stratigraphic relationships are unclear. All are intruded by biotite granite that is locally porphyritic, and probably part of either the ~ 1.4 Ga Mount Evans batholith or the ~ 1.1 Ga Pikes Peak batholith. Detailed descriptions of units and maps can be found in Mahatma, 2019; Powell et al., 2022.

The Paleoproterozoic metamorphic rocks show millimeter- to half meter-scale isoclinal F_1 folds that deform original compositional layering and perhaps earlier foliations. Their orientations vary due to later folding. Poles to S_1 plot along a great circle, of which the pole is parallel to the F_2 fold hinge lines (Fig. 4a, b). Isoclinal to open, cm- to m-scale and northerly plunging F_2 folds fold S_1, which locally includes sillimanite. Mm-scale to cm-scale parasitic s- and z-folds are present on fold

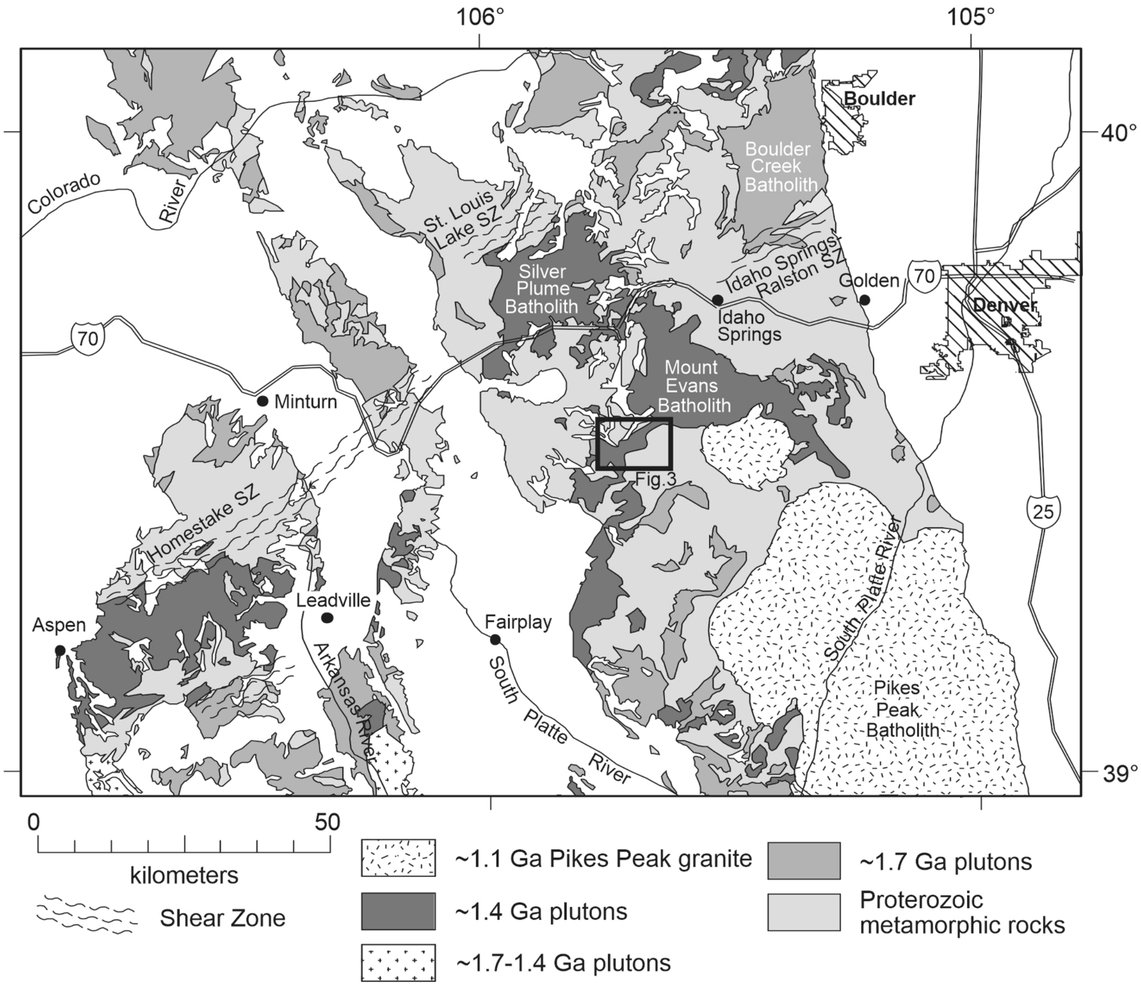

Fig. 2. Simplified geologic map of Proterozoic geology of central Colorado, modified after Shaw et al. (2002).

limbs. Poles to F_2 axial planes plot along a great circle suggesting a third generation of folds (F_3) plunging moderately to the NNE (Fig. 4c). However, F_3 folds were not observed in the field. Local F_4 folds are upright with shallowly east-plunging hinge lines. Mesoproterozoic granodiorite, and various types of fine- to coarse-grained granite, are largely undeformed but contain local flow foliations parallel to intrusive contacts.

4. Petrography of analyzed samples

One quartzite sample, and thirteen samples of biotite schist were selected for petrographic study and potential U–Pb zircon and monazite LA-ICPMS analysis. The quartzite (sample 336, unit Yqt, Figs. 3, 5) contains 94 % quartz grains, 4 % opaques that are most likely ilmenite (based on color and isotropy in reflected light) and magnetite (based on anisotropy in XPL under reflected light and cubic shape), 2 % apatite, and trace amounts of sericitized muscovite, and biotite, along with secondary chlorite replacing biotite, and zircon (Fig. 5c,d). Quartz grains shows irregularly shaped grain boundaries suggesting high-temperature grain boundary migration, overprinted by low-temperature recovery and recrystallization textures including undulose extinction, subgrain rotation recrystallization, and bulging recrystallization (Fig. 5d). The opaques are inclusions in quartz crystals and generally align with the S_1 foliation (Fig. 5c).

All thirteen thin sections from the biotite schist (unit Xbq, Fig. 3) show similar amphibolite facies metamorphic mineral assemblages with quartz, K-feldspar, biotite, and various amounts of sillimanite. The main S_1 foliation consists of biotite and sillimanite cleavage domains separated by quartz and feldspar microlithons, where sillimanite overgrows muscovite (Fig. 5e) that formed by the reaction of muscovite + quartz = sillimanite + K-feldspar + H_2O (Spear et al., 1999). The subsolidus breakdown of muscovite to K-feldspar implies mid-crustal pressures (4 kbar) (Johannes and Holtz, 2012) and the presence of sillimanite implies temperatures of 500–700 °C. Garnet is present in sample 281 and minor secondary muscovite overgrowing biotite is present in sample 332. A sillimanite-biotite foliation (S_1) is folded by F_2 folds, where biotite forms the S_2 axial planar foliation (Fig. 5f).

5. U–Pb LA-ICPMS data

5.1. U–Pb LA-ICPMS methods

We collected 20 kg of quartzite for U–Pb detrital zircon analysis. At the Colorado School of Mines, conventional crushing and grinding methods, a Wilfley™ wet-shaking table, heavy liquids (lithium metatungstate; specific gravity of 2.95), and a Frantz™ magnetic separator were used to concentrate the heavy, non-magnetic mineral fraction from the quartzite. Zircon grains were then picked under a binocular microscope, and mounted in epoxy at the U.S. Geological Survey in Denver, Colorado. The mount was ground to approximately half thickness of the grains and polished to expose the internal portions of the zircon. Cathodoluminescence (CL) images were acquired using a JEOL 5800 scanning electron microscope at the U.S. Geological Survey Microbeam Laboratory in Denver, Colorado.

Thirteen oriented thin sections of biotite schist were cut perpendicular to the second generation of regional folds. All thin sections were

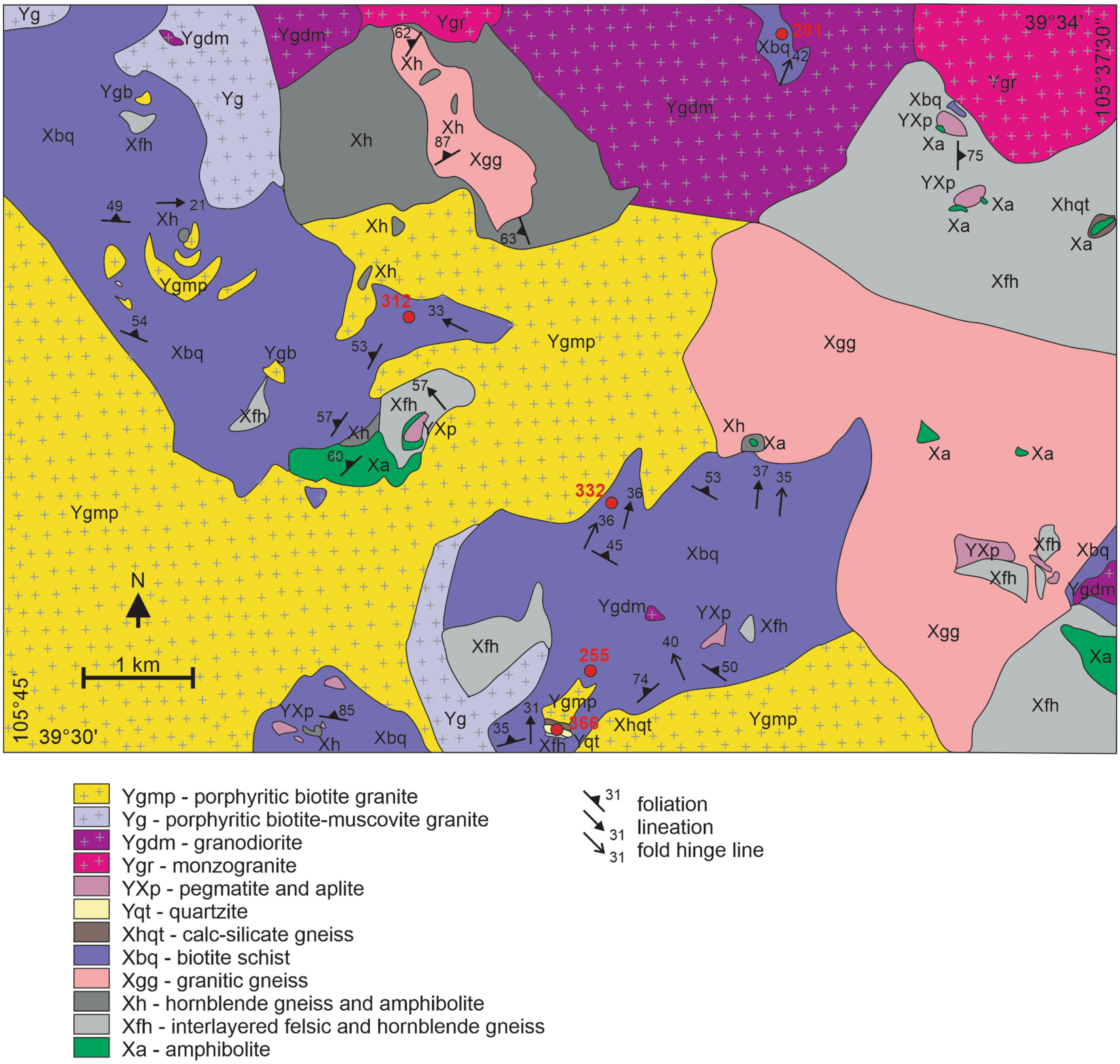

Fig. 3. Simplified geologic map of the southern half of the Mount Evans 7.5-minute quadrangle with representative structural data and sample locations (see Supplementary data 2 for coordinates). Modified after Mahatma (2019).

examined using optical microscopy. Ten were also evaluated using Automated Mineralogy in the Department of Geology and Geological Engineering at the Colorado School of Mines. Thin sections were first carbon coated then loaded into the TESCAN-VEGA-3 Model LMU VP Scanning Electron Microscope (SEM). Monazite for U–Pb LA-ICPMS analysis was identified using a bright phase search scan at a 2 μm beam stepping interval. Four biotite schist samples were then selected for backscattered electron (BSE) analysis, based on the alignment of monazite to microstructures, using a Mira3 high-resolution field emission SEM (FE-SEM) from TESCAN. To identify microstructural relationships of monazite and internal zonations, thin sections were scanned at a working distance of 10 mm using an acceleration voltage of 15 kV and a beam intensity of 11 pA.

All U–Pb geochronology on zircon from the quartzite and monazite from biotite schist was conducted at the U.S. Geological Survey Geology, Geophysics, and Geochemistry Science Center-Plasma Lab in Denver, CO. In situ-monazite U–Pb LA-ICPMS analyses were conducted using a Photon Machines Excite™ 193 nm ArF excimer laser coupled to a Nu Instruments AttoM high-resolution magnetic-sector inductively coupled plasma mass spectrometer in spot mode with a repetition rate of 5 Hz, laser energy of ~ 3 mJ, and an energy density of 4.11 J/cm^2. Nitrogen with flow rate of 5.5 mL/min was added to the sample stream to allow for significant reduction in ThO+/Th+ (<0.5 %) and improved the ionization of refractory Th (Hu et al., 2008). ^{202}Hg, ^{204}(Hg + Pb), ^{206}Pb, ^{207}Pb, ^{208}Pb, ^{235}U, and ^{238}U isotope mass peaks were measured. Raw data were reduced by using the Iolite™ 2.5 program (Paton et al., 2011). Monazite 44,069 (Aleinikoff et al., 2006) was used as an external reference material. The reference material was analyzed after every five spot analyses of monazite. LA-ICPMS zircon analysis was conducted using a procedure similar to that used for monazite analysis, but with a spot size of ~ 25 μm, and using the primary zircon reference material Temora2 (417 Ma; Black et al., 2004) and secondary reference materials

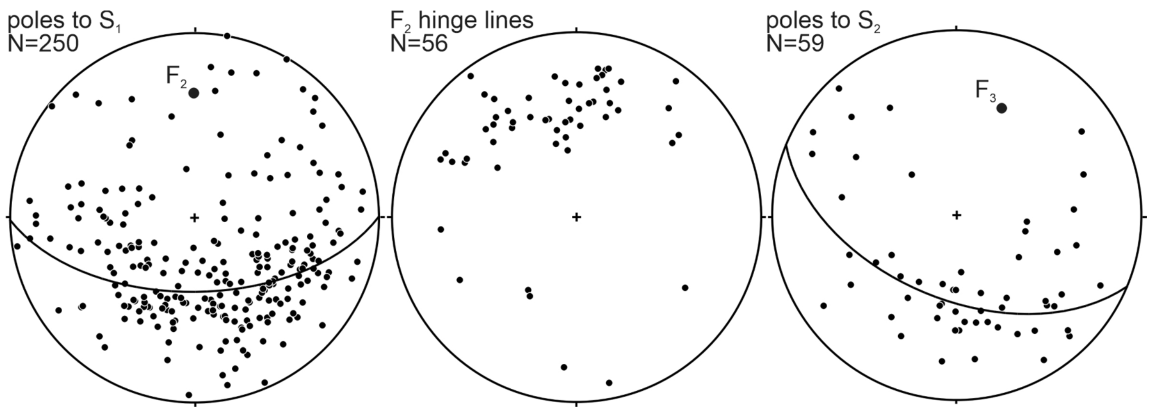

Fig. 4. Equal-area lower-hemisphere projection of structures in the study area. (a) Poles to S_1 foliation with best-fit great circle and F_2 fold axis indicated. (b) F_2 fold hinge lines. (c) Poles to S_2 foliation and F_2 axial planes with best-fit great circle and F_3 fold axis indicated.

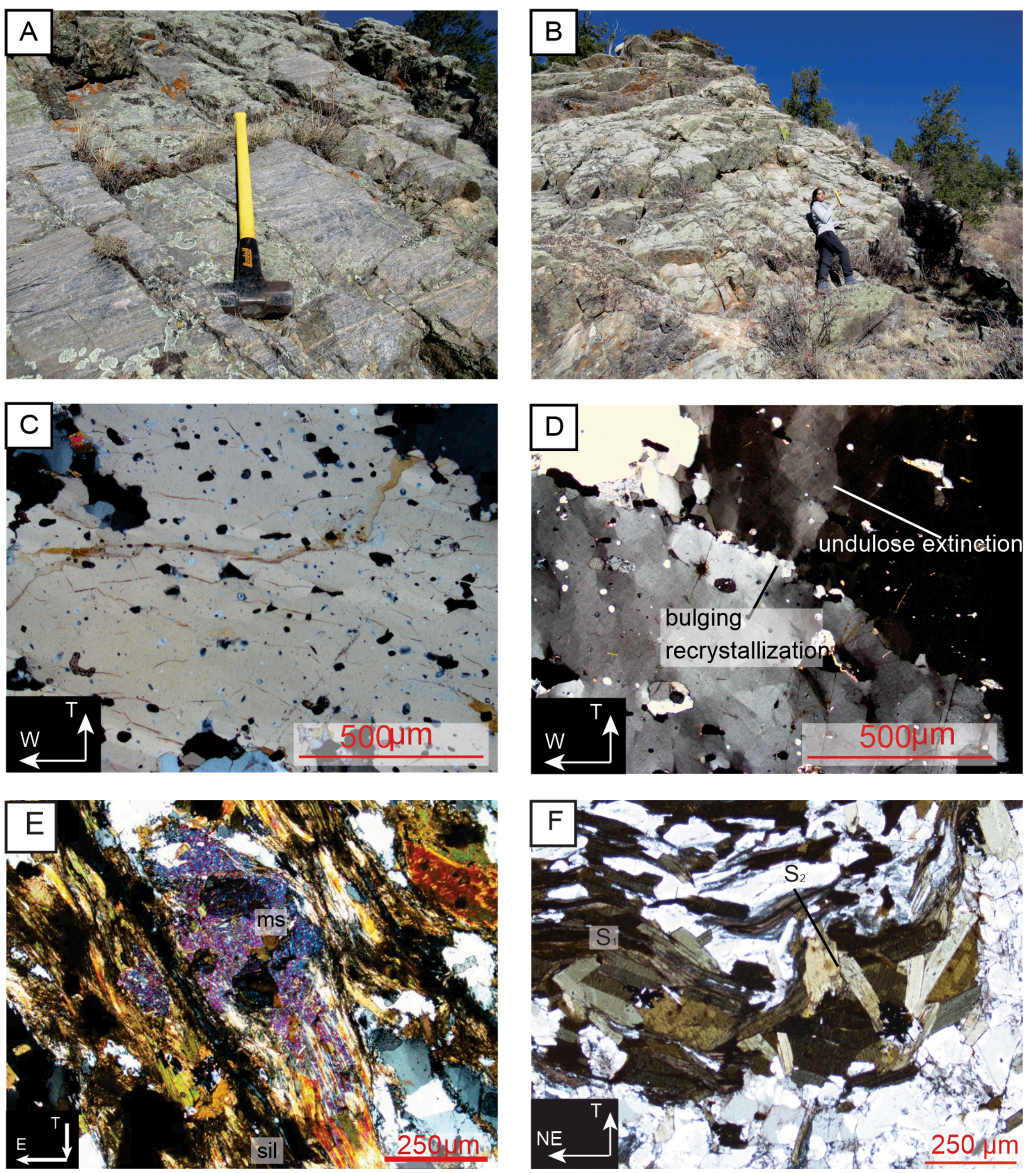

Fig. 5. (a, b) Field photographs of quartzite looking northeast. (c–f) Thin section images (mineral abbreviations are from Whitney and Evans, 2010). (c) Quartzite (sample 336) in PPL. (d) Quartz in the quartzite with bulging recrystallization, undulose extinction and subgrains in XPL. (e) Muscovite in sample 332 breaking down to sillimanite in XPL. (f) S_1 and S_2 in sample 312 (PPL).

FC-1 (1099 Ma; Paces and Miller, 1993), and Plešovice (337 Ma; Sláma et al., 2008). All raw data from the monazite and the zircon were reduced using Iolite™ 2.5 (Paton et al., 2011), and then subsequently interpreted and plotted using Isoplot4.15 (Ludwig, 2012). Only analyses<10 % discordant and with<10 % uncertainty were used for both the zircon and the monazite data interpretation. All ages reported are weighted averages of $^{207}Pb/^{206}Pb$ ages at the 2σ uncertainty level unless otherwise stated.

5.2. U–Pb LA-ICPMS results

Detrital zircon grains are euhedral to anhedral, 25–270 μm in length and with aspect ratios of 1:1 to 1:3 (Supplementary data 1). Some grains display cores and overgrowths while others show concentric and oscillatory zoning. Some grains are unzoned. Unzoned anhedral grains and overgrowths may reflect metamorphic zircon. Of 119 zircon U–Pb LA-ICPMS analyses in the quartzite (sample 366), 85 are concordant (Fig. 6a,b; Supplementary data 2). The $^{207}Pb/^{206}Pb$ dates can be divided into 1904 ± 57 Ma (MSWD = 0.21; N = 3) ~ 1809–1607 Ma (N = 54), 1558 ± 32 Ma (MSWD = 0.070; N = 5) and ~ 1489–1376 Ma (N = 23) populations, where weighted averages of $^{207}Pb/^{206}Pb$ ages are only used for populations with identical ages (Fig. 6c). The ~ 1809–1607 Ma and ~ 1489–1376 Ma age populations reflect spreads of ages instead of single age populations (Fig. 6c). The youngest zircon population is the ~ 1489–1376 Ma population, and the maximum depositional age may be interpreted as the 1427 ± 14 Ma weighted average of $^{207}Pb/^{206}Pb$ ages of that group (MSWD = 1.6; N = 23) or as the 1392 ± 17 Ma average of the youngest six grains within that group (MSWD = 0.32; N = 6). Th/U ratios for zircon < 1.5 Ga are < 0.1 while for older zircon they < 0.1 to 1.24 (Fig. 6d; Supplementary data 2).

In schist sample 255, 21 of 30 analyses from 12 monazite grains are concordant (Fig. 7a, Supplementary data 1, 2). The $^{207}Pb/^{206}Pb$ ages range from 1663 ± 38 Ma to 1398 ± 40 Ma. Data can be divided in a 1663 ± 38 Ma to 1515 ± 34 Ma continuous growth group and a younger group with a weighted average of $^{207}Pb/^{206}Pb$ ages of 1425 ± 14 Ma (MSWD = 1.5; N = 8). Except for grain 255_1, all grains analyzed are anhedral to subhedral and located within quartz and biotite grains (Supplementary data 1), and aligned along the S_1 foliation that is refolded by the N–S trending F_2 folds (Fig. 8a,b),. Grain 255_1 is a large anhedral inclusion in quartz, and yielded a $^{207}Pb/^{206}Pb$ age of 1403 ± 32 Ma (Supplementary data 1, 2). No relationship was found between grain size and age, or between age and relationship with adjacent minerals. Five grains yielded multiple ages (255_24, 255_25, 255_29, 255_34, 255_5) (Supplementary data 1, 2). However, none of these grains exhibited core and rims in BSE.

Twenty-three analyses from 11 monazite grains in sample 312 yielded 17 concordant dates between 1652 ± 38 Ma and 1396 ± 35 Ma (Supplementary data 1, 2). Data can be separated into two groups (Fig. 7c,d). The oldest reflects continuous growth between 1652 ± 38 Ma and 1498 ± 35 Ma. The younger group yielded a weighted average of $^{207}Pb/^{206}Pb$ ages of 1425 ± 13 Ma (MSWD = 1.4; N = 14). All monazite grains are anhedral to subhedral. Four grains (312_5, 312_40, 312_41, 312_56) are aligned with S_1, four (312_1, 312_47, 312_36, 312_54) are inclusions in biotite and quartz, and three (312_9, 312_23, 312_11) are elongate subparallel to S_2, but not along an S_2 foliation plane (Supplementary data 1). Grain 312_11 is more poikiloblastic than others (Supplementary data 1). No relationships were found between age and grain size, age and metamorphic assemblage, or age and textural setting. Multiple analyses from single grains yielded similar $^{207}Pb/^{206}Pb$ ages.

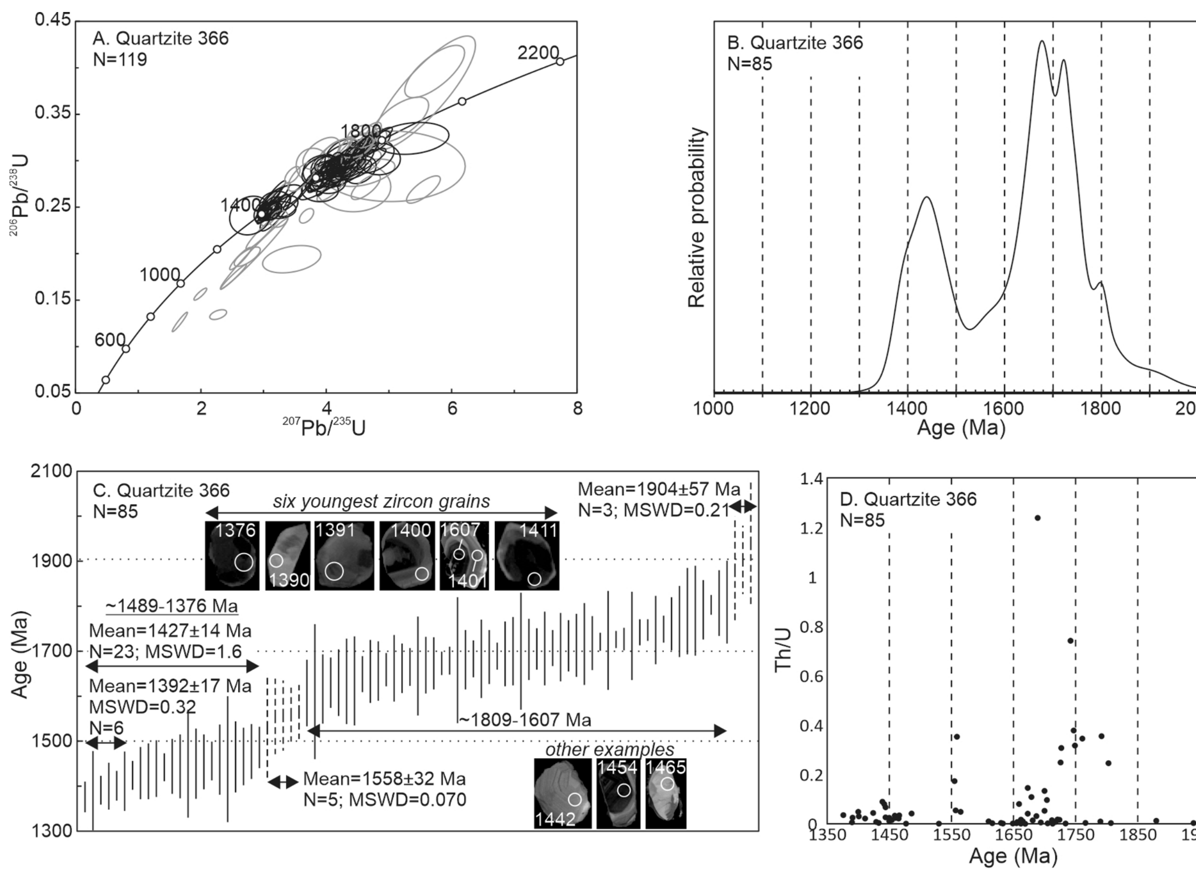

Fig. 6. U–Pb LA-ICPMS zircon data from a quartzite (sample 366; Fig. 3). (a) Error ellipses are 2σ and data that are > 10 % discordant gray. (b) Relative probability diagram showing concordant data. (c) Float bar chart with weighted averages of $^{207}Pb/^{206}Pb$ ages for concordant data, and representative zircon cathodoluminescence images. (d) Th/U ratio versus age plot.

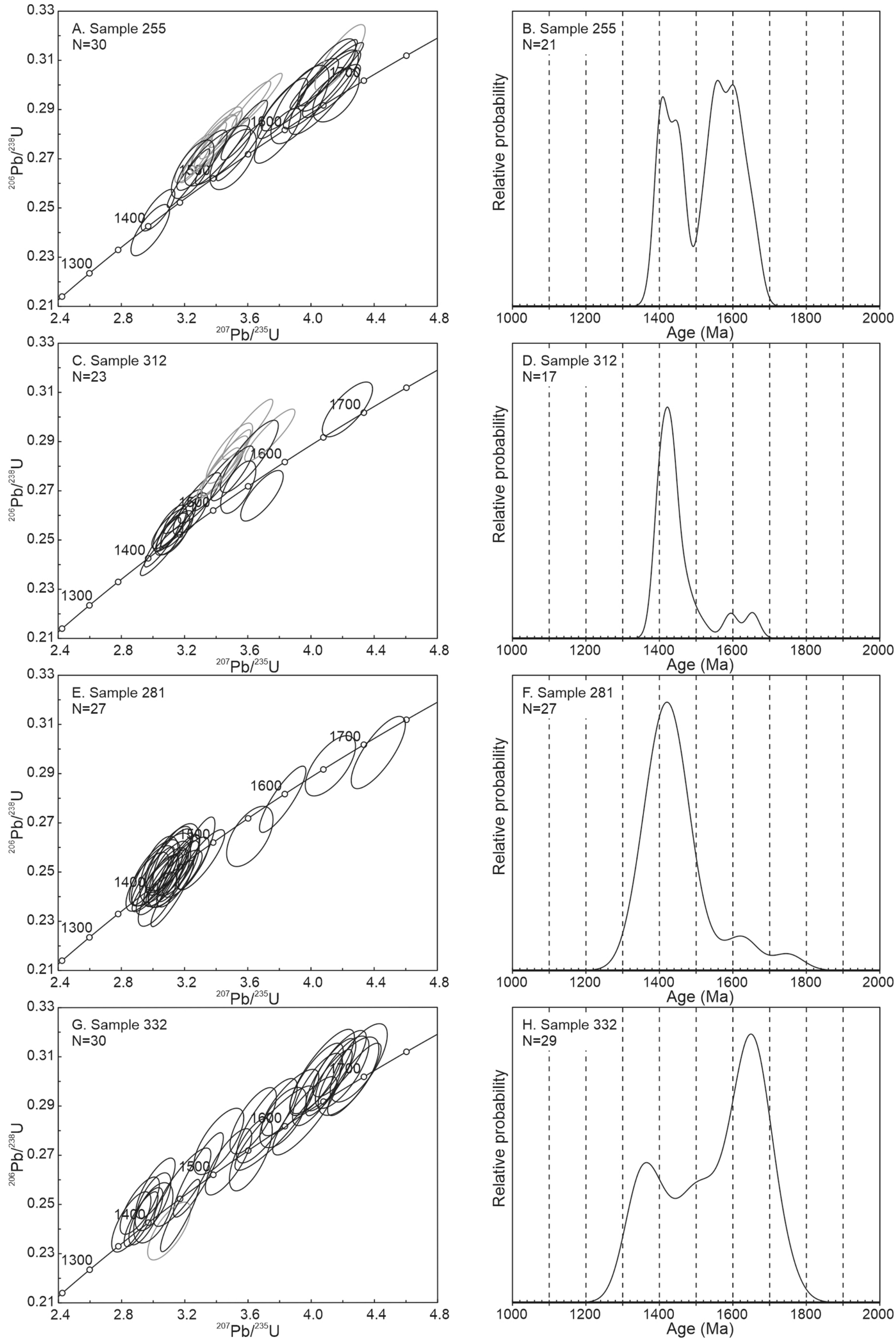

Fig. 7. U–Pb LA-ICPMS monazite data for the biotite schist samples. The concordia diagrams show 2σ error ellipses. Data that are > 10 % discordant in gray. Concordia diagrams (a,c,e,g) and relative probability diagrams (b,d,f,h) are for samples 255, 312, 281 and 332, respectively.

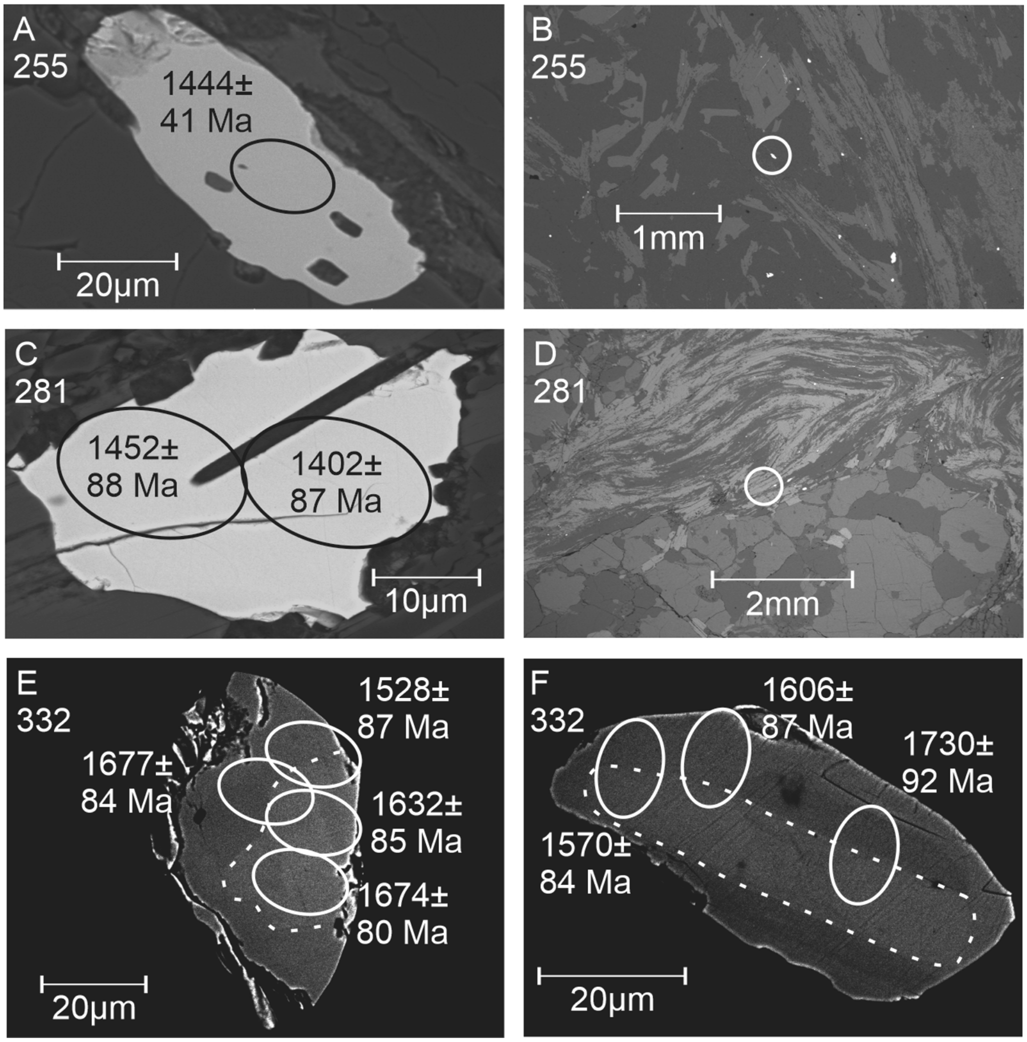

Fig. 8. BSE images showing representative textural relationships of dated monazite. (a, b) Grain 255_7 is an elongated anhedral grain aligned with foliation that has been refolded by N-trending F_2 folds. (c, d) Grain 281_n58 is an elongated anhedral grain aligned with foliation that has been refolded by N-trending F_2 folds. (e, f) High contrast BSE image of grains 332_25 and 332_9 showing cored and rims.

In sample 281, 27 spot analyses from 11 monazite grains are all concordant (6e,f; Supplementary data 1, 2) between 1749 ± 84 Ma and 1347 ± 95 Ma. Data show a spread between 1749 ± 84 Ma and 1533 ± 90 Ma, and a cluster with a weighted average of $^{207}Pb/^{206}Pb$ ages of 1425 ± 13 Ma (MSWD of 0.74; N = 23). The grains in this sample are mostly anhedral, and about half the grains are more poikiloblastic or more broken than in the other samples (Supplementary data 1). One grain (281_17) is an inclusion in garnet and yielded ages $^{207}Pb/^{206}Pb$ ages of 1416 ± 85 Ma and 1355 ± 86 Ma, two (281_10, 281_1) are adjacent to garnet, five (281_20, 281_5, 281_3, 281_33, 281_27) are inclusions in biotite or quartz, and three (281_n58, 281_25, 281_40) are aligned along a refolded S_1 foliation (Fig. 8c,d; Supplementary data 1). Generally, ages obtained from the same grain yielded similar $^{207}Pb/^{206}Pb$ ages, with the exception of one grain (281_5), which displayed zoning (Supplementary data 1). Analyses 281_5.3, 281_5.2 and 281_5.1 yielded $^{207}Pb/^{206}Pb$ ages of 1533 ± 90 Ma, 1425 ± 88 Ma and 1370 ± 86 Ma, respectively, representing successive growth stages.

Sample 332 yielded 29 concordant analyses out of 30 analyses from 10 monazite grains (Fig. 7g,h; Supplementary data 1, 2). These analyses can be divided into three age groups (Fig. 7h). The oldest two groups yielded weighted averages of $^{207}Pb/^{206}Pb$ ages of 1727 ± 62 Ma (MSWD = 0.0064; N = 2) and 1646 ± 23 Ma (MSWD = 0.36; N = 13). A third group suggests continuous growth between 1570 ± 84 Ma and 1334 ± 85 Ma (Fig. 7h). Monazite from this sample is anhedral to subhedral (Fig. 8; Supplementary data 1). Eight grains (332_5, 332_4, 332_19, 332_9, 332_25, 332_4, 332_1, 332_35) are aligned along the foliation, and two (332_8, 332_7) are in inclusions in biotite (Supplementary data 1). In five grains (332_19, 332_25, 332_4, 332_5, 332_9) more than one age population was represented, and only two of these (332_25, 332_9; Fig. 8e,f) show overgrowths of ~ 1.57 and ~ 1.53 Ga (Supplementary data 1, 2).

Combined data from the four samples show four age populations (Fig. 9). The oldest yielded a weighted average of $^{207}Pb/^{206}Pb$ ages of 1735 ± 50 Ma (MSWD = 0.09; N = 3), followed by a spread of ages between ~ 1677 Ma and ~ 1473 Ma, a cluster of analyses with a weighted average of $^{207}Pb/^{206}Pb$ ages of 1424 ± 8 Ma (MSWD = 0.77; N = 38) and another spread of ages between ~ 1392 Ma and ~ 1334 Ma. Fig. 9a shows that, while both monazite and zircon show Paleoproterozoic and Mesoproterozoic age populations, these are each younger for monazite than for zircon. Only monazite yielded ~ 1.39–1.33 Ga ages. The significance of these ages is discussed in Section 7.

6. Regional data compilation

In order to interpret the data in a regional context, depositional, metamorphic, and igneous ages were compiled and combined with U–Pb monazite and zircon data from relevant areas in Colorado, New Mexico, and Arizona. These are summarized below and in Fig. 10. In northern

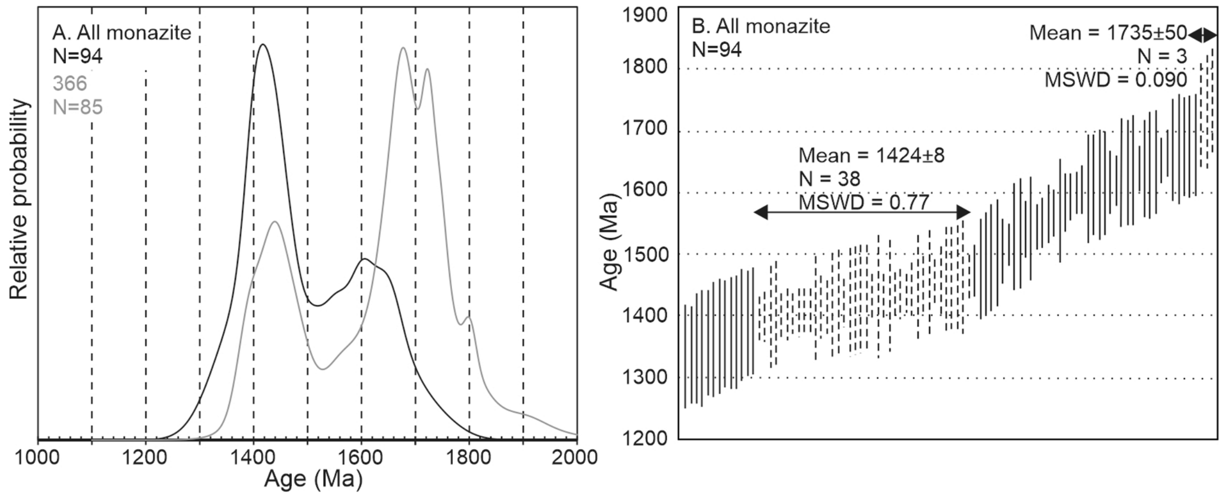

Fig. 9. (a) Relative probability diagram showing all monazite data from the biotite schist samples (black) and the quartzite (gray). (b) Float bar chart of $^{207}Pb/^{206}Pb$ ages for < 10 % discordant monazite spots from all biotite schist samples.

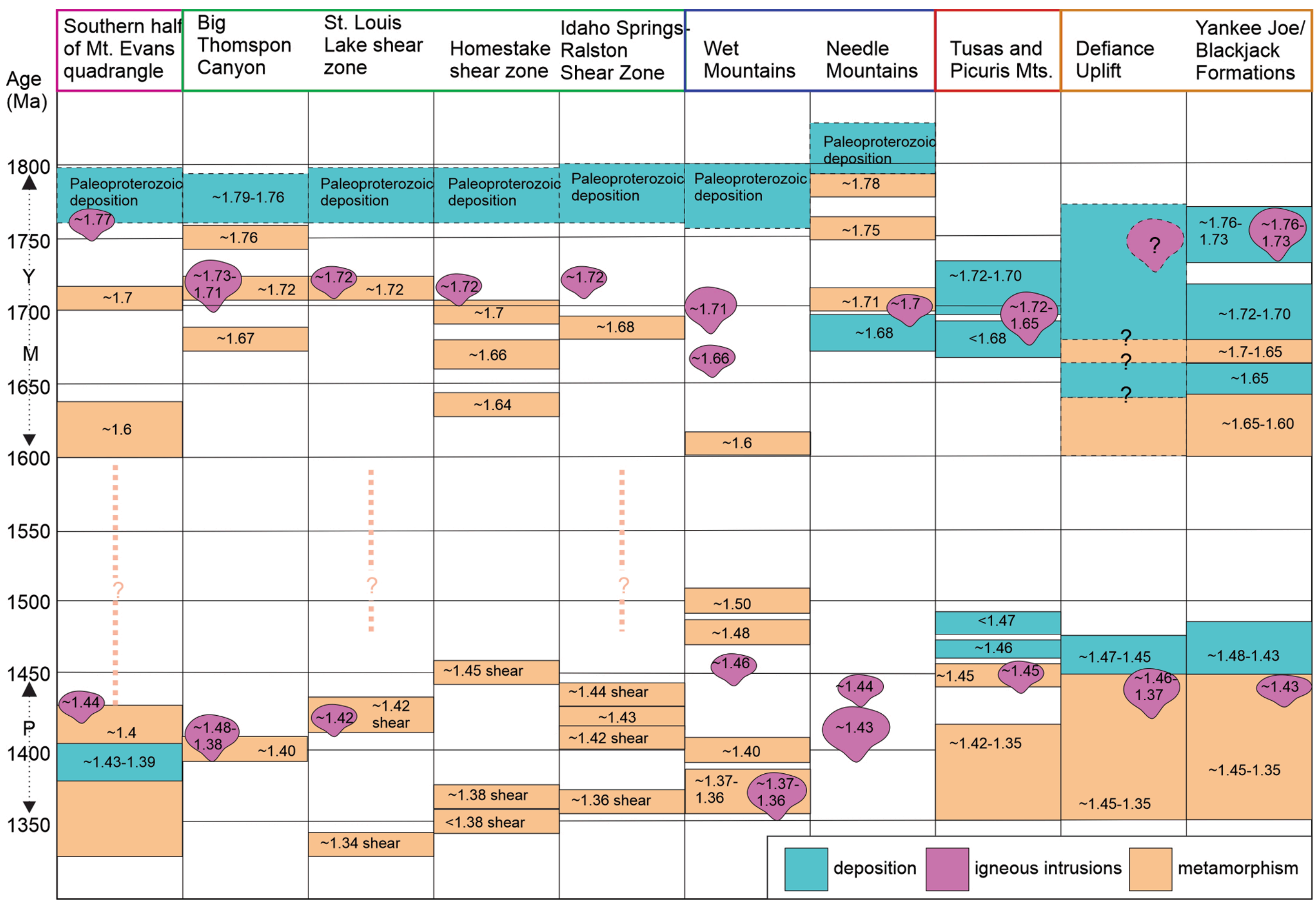

Fig. 10. Overview of Paleo- and Mesoproterozoic rock deposition (blue), metamorphism (light orange), and intrusion (pink) in Colorado, New Mexico, and Arizona. Color of boxes around headers reflects colors used in Fig. 1. Dotted arrows to the left of the diagram indicate the approximate extents of the Yavapai (Y), Mazatzal (M) and Picuris (P) tectonic events. (For interpretation of the references to color in this figure legend, the reader is referred to the web version of this article.)

Colorado, in Big Thompson Canyon (Figs. 1, 10), the oldest rocks include the Big Thompson metamorphic suite, which are predominately metasedimentary and metavolcanic rocks. Sensitive high-resolution ion microprobe (SHRIMP) U–Pb zircon crystallization ages from interlayered metavolcanic rocks are ~ 1.79–1.76 Ga (Premo et al., 2007). U–Pb zircon data from the metasedimentary rocks yielded a maximum depositional age of ~ 1.76 Ga (Selverstone et al., 2000). Deformation and metamorphism occurred at ~ 1.76 Ga, ~1.72 Ga and ~ 1.67 Ga, based on in situ microprobe monazite U–Th–Pb analyses (Shah and Bell, 2012), and coeval emplacement of the calc-alkaline Routt Plutonic Suite occurred at ~ 1.7 Ga (Tweto, 1987). Deformation involved ENE-trending F_1 isoclinal folds overprinted by east-trending, non-pervasive

F_2 folds, and open to tight northeast-trending F_3 folds (Mahan et al., 2013, and references therein). At ~ 1.4 Ga, the Berthoud Plutonic Suite was emplaced (Tweto, 1987). $^{40}Ar/^{39}Ar$ data show resetting of biotite and muscovite and partial resetting of hornblende at ~ 1.4 Ga in metaigneous rocks (Shaw et al., 1999). In situ microprobe U–Th–Pb ages of monazite inclusions in andalusite and cordierite porphyroblasts in metasedimentary rocks are ~ 1.4 Ga (Shah and Bell, 2012), indicating deformation and metamorphism at that time.

The St. Louis Lake Shear zone records a complex history of tectonism and syntectonic plutonism (Figs. 1, 2, 10). Paleoproterozoic metamorphic rocks were intruded by the Boulder Creek granodiorite at ~ 1.72 Ga (McCoy, 2001). In situ microprobe U–Th–Pb monazite ages reveal metamorphism at ~ 1.72 Ga. Upper amphibolite facies metamorphism, D_1 isoclinal folds, and D_2 folds with northeast-trending axial planes occurred at that time (McCoy, 2001; McCoy et al., 2005). Mylonites formed during emplacement of the ~ 1.42 Ga Silver Plume Granite (Hedge, 1969) and continued deformation resulted in ~ 1.34 Ga ultramylonites (McCoy, 2001).

Along the Homestake Shear Zone in central Colorado (Figs. 1, 2, 10), in situ electron microprobe monazite U–Th–Pb dates from biotite gneiss and migmatite show that Paleoproterozoic sedimentary rocks underwent repeated metamorphism at ~ 1.7 Ga, ~1.66 Ga, and ~ 1.64 Ga (McCoy, 2001; McCoy et al., 2005). Isoclinal D_1 folds and open to isoclinal northeast-striking D_2 folds were overprinted by lower temperature mylonites at ~ 1.45 Ga and ultramylonites at and after ~ 1.38 Ga based on in situ electron microprobe U–Th–Pb monazite ages (McCoy, 2001).

Adjacent to the Idaho Springs–Ralston shear zone (Figs. 1, 2, 10), Paleoproterozoic rocks include metasedimentary units and the ~ 1.72 Ga Boulder Creek granodiorite/quartz monzonite (Premo and Fanning, 2000; Jones and Thrane, 2012). Metamorphism started at ~ 1.68 Ga based on in situ electron microprobe and LA-ICPMS U–Th–Pb monazite ages (McCoy, 2001; Lytle, 2016). D_1 isoclinal folds, tentatively interpreted as SE-verging and upper amphibolite facies metamorphism, are interpreted as having occurred at that time (Lytle, 2016). Open to close, cm–m-scale shallowly northeast- plunging D_2 folds, and a shallowly northeast-plunging D_3 syncline with a steeply northwest-dipping axial plane developed at ~ 1.43 Ga, based on in situ LA-ICPMS monazite U–Pb geochronology (Lytle, 2016). Lower temperature mylonites and ultramylonites formed at ~ 1.44–1.36 Ga, based on in situ U–Pb monazite geochronology (McCoy et al., 2005; Lytle, 2016).

In the Wet Mountains in southern Colorado (Figs. 1, 10), Paleoproterozoic (?) metasedimentary rocks, felsic gneiss, migmatite and amphibolite contain upper amphibolite to granulite facies metamorphic mineral assemblages (Siddoway et al., 2000; Jones et al., 2010b; Levine et al., 2013). Plutonism occurred at ~ 1.71–1.66 Ga and ~ 1.47–1.36 Ga (Bickford et al., 1989; Jones et al., 2010b), metamorphism may have been as early as ~ 1.6 and ~ 1.5–1.48 Ga based on Lu–Hf garnet geochronology (Aronoff, 2016). NNW-directed shortening and metamorphism occurred at ~ 1.44–1.40 Ga based on U–Pb zircon and monazite geochronology (Siddoway et al., 2002; Jones et al., 2010b; Daniel et al., 2013a).

In the Needle Mountains in southwest Colorado (Figs. 1, 10) Paleoproterozoic metasedimentary and metavolcanic rocks were deformed and metamorphosed at ~ 1.75 Ga based on Lu–Hf garnet geochronology (Aronoff, 2016). These rocks were subsequently intruded by ~ 1.7 Ga and ~ 1.44–1.43 Ga plutons (Gonzales and Van Schmus, 2007; Keller and Schoene, 2015), some of the latter are deformed by northerly directed shortening (Gonzales et al., 1996; Gonzales and Van Schmus, 2007).

In the Tusas and Picuris Mountains of northern New Mexico (Figs. 1, 10), metasedimentary rocks were deposited during the Paleoproterozoic and the Mesoproterozoic (~1.49–1.45 Ga; Jones et al., 2011; Daniel et al., 2013a,b). Mesoproterozoic detrital zircon grains are present in the Marqueñas and Pilar and Piedra Lumbre Formations in the Picuris Mountains of northern New Mexico (Fig. 1; Jones et al., 2011; Daniel et al., 2013b). The youngest zircon age population in the Marqueñas Formation is ~ 1.46 Ga (Jones et al., 2011; Daniel et al., 2013a,b). Although the minimum age of deposition is not well constrained, it has been interpreted to be ~ 1.43 Ga based on regional metamorphism and deformation (Jones et al., 2011). The Pilar and Piedra Lumbre Formations include interbedded sedimentary and volcanic rocks deposited between ~ 1.49 Ga and ~ 1.45 Ga, based on the presence of ~ 1.49 Ga zircon in a metatuff and the relative stratigraphic position with the Marqueñas Formation (Daniel et al., 2013b). Dates from the Tusas and Picuris Mountains also reveal a significant population of ~ 1.5 Ga zircons, interpreted as exotic detritus from Australia or Antarctica (Jones et al., 2011; Daniel et al., 2013a,b). Lu–Hf ages for garnet and in situ electron microprobe U–Th–Pb ages for monazite reveal that metamorphism in this area is ~ 1.46–1.35 Ga (Kopera et al., 2002; Daniel and Pyle, 2006; Aronoff, 2016; Aronoff et al., 2016). This amphibolite facies metamorphism is interpreted as relatively low-pressure intermediate-temperature (4 kbar, 530–590 °C), based on the presence of kyanite, sillimanite, and andalusite (Daniel and Pyle, 2016; Aronoff, 2016). Based on porphyroblast-matrix textures, three generations of deformation occurred between ~ 1.45 Ga and ~ 1.35 Ga and resulted primarily from regional northerly-directed shortening (Aronoff, 2016; Aronoff et al., 2016).

The Defiance uplift in eastern Arizona (Figs. 1, 10) is a west-verging basement-cored monocline exposing small outcrops of quartzite in four canyons. The Defiance quartzite consists of medium-grained quartz arenite with subordinate subarkose and arkose, without a lower contact exposed. Based on nearby outcrops, the Defiance quartzite likely rests nonconformably on Paleoproterozoic plutons (Doe et al., 2012). LA-ICPMS U–Pb zircon analysis of the Defiance quartzite yielded a youngest detrital zircon age population of ~ 1.47 Ga (Doe et al., 2013). The depositional age of this quartzite is constrained to ~ 1.47–1.45 Ga based on the absence of 1.45–1.35 Ga detrital zircon populations in an area where abundant ~ 1.46–1.37 Ga granites are exposed (Doe et al., 2013; Karlstrom et al, 2004). The quartzite also contains a large population of ~ 1.5 Ga zircons interpreted as exotic detritus from adjacent continents such as Australia or Antarctica, and was subsequently weakly deformed and weakly metamorphosed at ~ 1.45–1.35 Ga based on regional correlation.

The oldest rocks of the northern Tonto Basin in the Mazatzal Mountains and Chino Valley to the northwest in central Arizona (Fig. 1) are ~ 1.76–1.73 Ga ophiolitic and arc plutonic rocks, overlain by ~ 1.73–1.70 Ga metasedimentary and metavolcanic rocks (Dann, 1997; Conway and Silver, 1989; Spencer et al., 2016). This succession is overlain unconformably by the ~ 1.66–1.60 Ga Mazatzal Group and the ~ 1.57 Hopi Springs Formation (Doe and Daniel, 2019). A metapelite disconformably overlying the Four Peaks Quartzite within the Four Peaks synform of the southern Mazatzal Mountains yielded a youngest detrital zircon age population ~ 1.58 Ga. The Four Peaks Quartzite rests on ~ 1.66 Ga rhyolite (Mako et al., 2015).

In the upper Salt River Canyon of the southern Tonto Basin, the Early Mesoproterozoic Yankee Joe Group overlies the Paleoproterozoic White Ledges and ~ 1.66 Ga Redmond Formations. The Yankee Joe Group consists of weakly metamorphosed shale interbedded by arkosic sandstone and siltstone of the Yankee Joe Formation, grading upward into the quartzite-rich Blackjack Formation (Doe et al., 2012, 2013; Figs. 1, 10). The depositional age of the Yankee Joe Group is constrained between the ~ 1.47 Ga youngest zircon age population in the Blackjack Formation and the ~ 1444 Ma Ruin granite that intrudes the upper Blackjack Formation (Fig. 10; Doe and Daniel, 2019; Doe et al., 2012, 2013). The Yankee Joe and Blackjack formations each contain a large population of ~ 1.5 Ga zircon grains, which may have included local sources as close as the McDowell Mountains near Phoenix, Arizona (Skotnicki and Gruber, 2019) or as far away as Australia or Antarctica (Doe et al., 2012, 2013). The Paleoproterozoic and Early Mesoproterozoic successions in the upper Salt River Canyon are unconformably overlain by the Middle Proterozoic Apache Group quartzite and conglomerate.

All of these localities in central Arizona are deformed by northwest-directed shortening attributed to the Mazatzal orogeny and now known to have occurred at ~ 1.47–1.44 Ga (Doe and Daniel, 2019). Similarly, Ferguson et al. (2004) reported northwest-directed shortening in the synkinematic ~ 1.4 Ga Boriana Canyon Pluton, in the Hualapai Mountains of northwestern Arizona (Fig. 1).

7. Discussion

7.1. Data interpretation

Field mapping reveals evidence for at least four deformation events in the southern half of the Mt. Evans quadrangle. D_1 isoclinal folds are overprinted by moderately north-plunging F_2 folds and moderately NNE-plunging F_3 folds. The fourth deformation event consists of local open upright east-trending folds. Metamorphism occurred at mid-crustal pressures of ~ 4 kbar and temperatures of 500–700 °C.

Detrital zircon in the quartzite yielded ~ 1.90 Ga, ~1.81–1.61 Ga, ~1.56 Ga and ~ 1.49–1.38 Ga populations. Grains of the ~ 1.56 Ga population displayed cores and rims and the ages may be a result of the mixing of age domains, which is further discussed below. In general, all Th/U ratios for ~ 1.49–1.38 Ga zircon are < 0.1, while Th/U ratios for older zircon (~1.90–1.56 Ga) are mainly < 0.1 but also > 0.1 (Fig. 6d; Mahatma, 2019; Supplementary data 2). If all the zircon is detrital, the maximum age of deposition may be interpreted as the 1427 ± 14 Ma weighted average of $^{207}Pb/^{206}Pb$ ages of the ~ 1.49–1.38 Ga zircon population (N = 23), or the 1392 ± 17 Ma average age of the youngest six grains within that group. It is alternatively possible that the youngest age population is metamorphic or hydrothermal, and that the quartzite is Paleoproterozoic as numerous others in the southwestern U.S. (e.g., Jones and Thrane, 2012; Jones et al., 2015).

Th/U ratios < 0.1 in the ~ 1.49–1.38 Ga zircon population and part of the older populations may be an indication of metamorphic zircon. However, they may alternatively be a result of competition for Th with other high Th minerals such as monazite and allanite (Möller et al., 2003; Yakymchuk et al., 2018), making Th/U ratios alone not a reliable indicator for zircon origin. The variation in Th/U in zircon is a result of open system behavior and can occur during the formation of magmatic, metamorphic, and hydrothermal zircon (Möller et al., 2003; Lopez-Sanchez et al., 2015; Yakymchuk et al., 2018). Therefore, characterizing zircon as metamorphic solely based on Th/U ratios can lead to misinterpretation (Möller et al., 2003).

Most of the zircon grains of all age populations in sample 366 show typical concentric or sector zoning, and subrounded morphologies that are typical for detrital zircon (Fig. 6c; Mahatma, 2019; Supplementary data 1). There is no evidence for partial melt in the quartzite and, therefore, these zoned grains are more likely to have formed in igneous or partially melted source rocks prior to erosion and deposition, as opposed to within the quartzite during metamorphism. Some ~ 1.81–1.61 Ga and ~ 1.49–1.38 Ga zircon are anhedral and unzoned or have unzoned overgrowths, a texture typical of metamorphic zircon (e.g. ~ 1390 Ma grain in Fig. 6c; Corfu et al., 2003; Supplementary data 1). Some or all of this metamorphic zircon may have grown in another rock prior to erosion and deposition into the protolith/sediment of the quartzite as detrital zircon. Both zoned and unzoned zircon occur in various age populations, and both types show low Th/U ratios (Fig. 6c; Mahatma, 2019). Some ~ 1.49–1.38 Ga zircon show rims that are too narrow to analyze (Fig. 6c; Supplementary data 1), indicating that metamorphism of the quartzite occurred after formation of the youngest age population.

It is possible that the youngest zircon age population is hydrothermal. Hydrothermal zircon precipitated from fluid or fluid-saturated melt, e.g. from nearby granitoid batholiths and intruding late granite of the Mount Evans and/or Pikes Peak batholiths, may exhibit structures that are typical of igneous zircons, such as oscillatory or sector zoning, or of metamorphic zircons (Fu et al., 2009; cf. Fig. 6c). However, no equivocal evidence for hydrothermal growth of zircon (cf. Schaltegger, 2007) in the quartzite was observed. Therefore, it is unlikely the zircon in the quartzite is hydrothermal.

In summary, the diversity in zircon morphologies and zoning, and the presence of narrow metamorphic overgrowths in all populations including the youngest one suggest that all analyzed zircon including the ~ 1.49–1.38 Ga population is detrital. The quartzite was metamorphosed after deposition, probably between ~ 1.39 Ga and ~ 1.33 Ga based on the youngest monazite population. Another possibility is that the ~ 1.49–1.38 Ga population reflects Pb loss of older zircon due to regional metamorphism and/or contact metamorphism. However, that would be expected to have resulted in a spread of data along a discordia chord between the main older ~ 1.81–1.61 Ga population and the ~ 1.49–1.38 Ga population, which is not observed.

Sources for the ~ 1.49–1.38 Ga youngest detrital zircon population may be the local 1442 ± 2 Ma Mt. Evans batholith, the 1424 ± 6 Ma Silver Plume batholith, and related intrusive rocks (Aleinikoff et al., 1993; Kellogg et al., 2008, cf. Premo, unpublished data, 2005), or more distal sources, including the ~ 1371–1362 Ma San Isabel pluton (Bickford et al., 1989; Cullers et al., 1992) or ~ 1435 Ma and ~ 1390 Ma granitic sills of the southern Wet Mountains (Jones et al., 2010b). The maturity of the quartzite, subrounded zircon morphologies, and the absence of conglomeratic parts may suggest that distal sources are more likely, but this remains inconclusive due to the small size of the exposure.

The ~ 1.56 Ga population may represent a detrital zircon population, or possibly a result of mixing of age domains or Pb loss. Potential ~ 1.6–1.5 Ga sources in western Laurentia include the 1.58–1.57 Ga orthogneiss of the Priest River complex in the northwestern United States, 1.60–1.59 Ga volcanic rocks and diabase in northwestern Canada (Doe et al., 2013, and references therein), a ~ 1.52 Ga ash layer in the Trampas group in New Mexico (Daniel et al., 2013b), a ~ 1.55 Ga ash-flow tuff and ~ 1.53 Ga granite in the McDowell Mountains in Arizona (Fig. 1; Skotnicki and Gruber, 2019), and possibly ~ 1.49 Ga igneous intrusions in Colorado that may be within uncertainty (Tweto, 1987), but these sources are rare. Similar detrital zircon ages occur in sedimentary rocks from the Defiance uplift, the Yankee Joe and Blackjack Formations of the upper Salt River Canyon, the Four Peaks area in Arizona, and the Tusas and Picuris Mountains in New Mexico (Daniel et al., 2013b; Doe et al., 2013; Mako et al., 2015). Interpreted sources are from formerly adjacent landmasses such as the East Antarctic craton, Australia, Siberia, or South China, where ~ 1.55 Ga zircons are common (Goodge et al., 2008; Doe et al., 2013). It has been suggested that some sedimentary basins in Laurentia formed between ~ 1.5 Ga and ~ 1.4 Ga (Jones et al., 2011, 2015; Doe et al., 2012). These basins received sediments from low relief rivers that deposited exotic detritus from formerly adjacent landmasses onto the Laurentian craton. These regions were also potential sources for the ~ 1.56 Ga zircon in the quartzite (Doe et al., 2012; Jones et al., 2015).

Monazite grains from the biotite schist yielded a small population of ~ 1.74 Ga, main ones of ~ 1.68–1.47 Ga and ~ 1.42 Ga, and a minor population of ~ 1.39–1.33 Ga (Fig. 9). The ~ 1.68–1.47 Ga population shows a ~ 1.60 Ga and a smaller ~ 1.54 Ga age peak (Fig. 9a). Metamorphic events affecting Laurentia between ~ 1.60 Ga and ~ 1.50 Ga are minimal (e.g. Doe et al., 2013). Therefore, it is more likely that the ~ 1.54 Ga peak may be the result of Pb loss in older monazite, or of the mixing of age domains in monazite. Monazite grains analyzed were aligned along S_1, S_2, or were inclusions in quartz, biotite, or garnet. No clear relationship between the age of monazite grains and textural setting within foliation generations was recognized. The monazite inclusion in garnet yielded ages of ~ 1.41 Ga and ~ 1.36 Ga, suggesting that the latest metamorphism occurred at or after ~ 1.36 Ga.

Based on these dates there are two possible interpretations for the depositional age of the biotite schist protolith. First, it is a Paleoproterozoic deposit, in which case the oldest ~ 1.74 Ga monazite population may be metamorphic or detrital. All other populations are then metamorphic and record subsequent periods of metamorphism. Alternatively, the biotite schist protolith may be Mesoproterozoic. In that case, all monazite would be detrital, except the youngest ~ 1.39–1.33 Ga and perhaps the ~ 1.42 Ga populations that represent metamorphism. Sources for Paleo- and/or Mesoproterozoic detrital monazite (if present) may be older local and regional metamorphic rocks. The ~ 1.39–1.33 Ga monazite population is, however, unlikely to be detrital, because there is no evidence for a younger metamorphic event that would have formed monazite, and because of the monazite inclusion in garnet with ~ 1.41 Ga and ~ 1.36 Ga ages.

In summary, the biotite schist is a Paleoproterozoic or early–mid-Mesoproterozoic deposit, while we interpret the quartzite protolith as having been deposited in the early–mid-Mesoproterozoic. Both were metamorphosed at ~ 1.39–1.33 Ga and perhaps earlier. The latest structures in the area are Mesoproterozoic, while the earliest deformation probably occurred in the Paleoproterozoic based on regional evidence. Mesoproterozoic deformation and metamorphism is consistent with the timing of the Picuris orogeny in northern New Mexico.

7.2. Tectonic implications

U–Pb zircon and monazite data summarized above were compiled and combined with data from this study (Fig. 11; Supplementary data 3; McCoy, 2001; Daniel and Pyle, 2006; Jessup et al., 2006; Jones et al., 2010b; Shah and Bell, 2012; Daniel et al., 2013b; Doe et al., 2013; Bickford et al., 2015; Mako et al., 2015; Aronoff, 2016; Lytle, 2016). Only $^{207}Pb/^{206}Pb$ dates that are < 10 % discordant are used in Fig. 11. Igneous and detrital zircon data revealed main age peaks at ~ 1.70 Ga and ~ 1.47 Ga, with a small detrital zircon population at ~ 1.56 Ga (Fig. 11a, b; this study; Jones et al., 2010b; Daniel et al., 2013b; Doe et al., 2013; Bickford et al., 2015; Mako et al., 2015; Aronoff, 2016). The ~ 1.70 Ga and ~ 1.47 Ga populations thus have numerous local and regional sources (Figs. 2, 11). Daniel et al. (2013b) and Doe et al. (2013) attributed ~ 1.56 Ga detrital zircon to exotic detritus, and later as a mixture of local and distant sources, as ~ 1525 Ma igneous and 1546 Ma volcanic rocks were discovered in the McDowell Mountains ~ 100 km west of the upper Salt River Canyon (Doe and Daniel, 2019; Skotnicki and Gruber, 2019).

Monazite $^{207}Pb/^{206}Pb$ ages from Colorado reveal ~ 1.69 Ga and ~ 1.40 Ga populations, and a smaller, but statistically valid ~ 1.51 Ga population (Fig. 11e, this study; McCoy, 2001; Jessup et al., 2006; Shah and Bell 2012; Lytle, 2016). A continuum of ages exists between ~ 1.58 Ga and ~ 1.46 Ga. These ages have previously been interpreted as mixed age domains (McCoy, 2001; Lytle, 2016). Monazite data from New Mexico show one age group at ~ 1.40 Ga (Fig. 11f; Daniel and Pyle, 2006). The youngest monazite ages in Colorado are younger than the youngest monazite ages in New Mexico.

In summary, the oldest rocks in New Mexico, Colorado, and Arizona were deposited and intruded during the Paleoproterozoic (~1.8–1.6 Ga). In Colorado and Arizona, these rocks experienced subsequent Paleoproterozoic metamorphism. Between ~ 1.6 Ga and ~ 1.5 Ga metamorphic and igneous activity diminished in Laurentia. Deposition

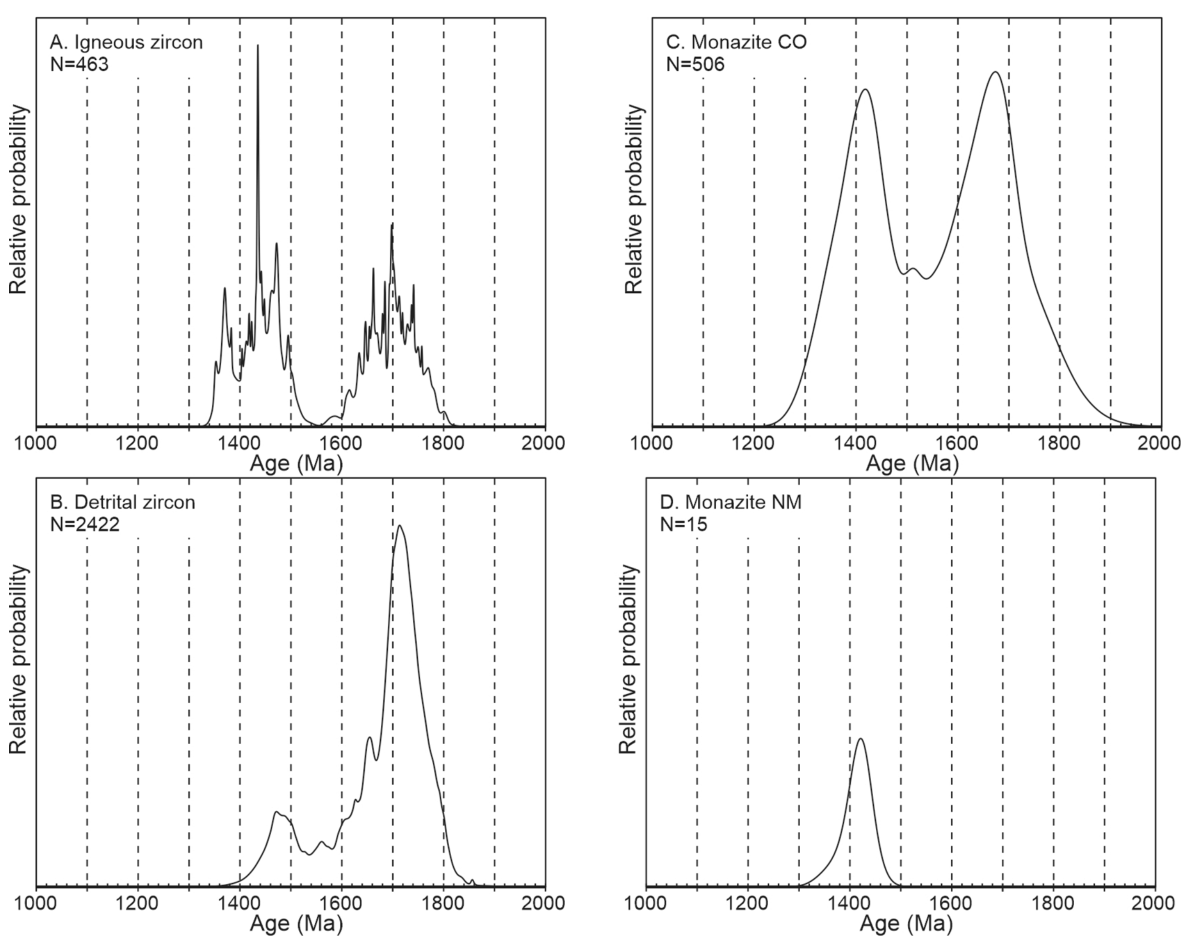

Fig. 11. Igneous and detrital zircon, and monazite data compiled from Colorado, New Mexico, and Arizona. Zircon is generally from quartzite, intrusive igneous rocks, and feldspathic schist and gneiss. Monazite is generally from biotite and felsic schist and gneiss. (a–d) Relative probability diagrams for all magmatic zircon from intrusive igneous rocks (data from Bickford et al., 2015; Aronoff, 2016), detrital zircon from metasedimentary rocks in New Mexico and Colorado (data compiled from this paper; Jones et al., 2010b; Daniel et al., 2013b; Doe et al., 2013; Mako et al., 2015), monazite from Colorado (data compiled from this paper; McCoy, 2001; Jessup et al., 2006; Shah and Bell 2012; Lytle, 2016), and monazite from New Mexico (data from Daniel and Pyle, 2006), respectively.

of Mesoproterozoic sedimentary basins in Arizona and New Mexico is constrained between ~ 1.47 Ga and ~ 1.43 Ga (Daniel et al., 2013b; Doe et al., 2013). In general, after early–mid-Mesoproterozoic sediment deposition, rocks in New Mexico, Colorado, and Arizona experienced a widespread lower greenschist to upper amphibolite facies metamorphic event that is generally constrained between ~ 1.48 Ga and ~ 1.35 Ga. Deposition of the quartzite of this study occurred after ~ 1.43 Ga, which is possibly later than in Arizona and New Mexico. The quartzite may have had local and/or distal sources, and may have been displaced after its deposition. It was buried and metamorphosed at ~ 1.39–1.33 Ga. The exact setting or location of the quartzite within the Picuris orogen, or the architecture of the Picuris orogeny in Colorado in general remain unclear.

The rocks in the Colorado Front Range are interpreted to have undergone metamorphism up to amphibolite facies during the Paleoproterozoic and the Mesoproterozoic (McCoy et al., 2005; Daniel and Pyle, 2006; Jones et al., 2010b; Shah and Bell 2012; Daniel et al., 2013b; Aronoff, 2016; Lytle, 2016). The rocks in Arizona experienced amphibolite facies metamorphism during the Paleoproterozoic, but only metamorphism as high as greenschist facies has been attributed to the Picuris orogeny (Mako et al., 2015). These contrasting metamorphic conditions may result from different locations within Paleoproterozoic and Mesoproterozoic orogenic belts. Furthermore, folds attributed to the Picuris orogeny trend broadly northeast in Arizona and west in New Mexico and NNW to NNE in the study area (Jones et al., 2010b; Shah and Bell, 2012; Daniel et al., 2013b; Doe et al., 2013; Doe, 2014 and references therein; Aronoff, 2016; Doe and Daniel, 2019) and are possibly a result of an orocline as proposed by Jones et al. (2010b), Shah and Bell (2012) and Aronoff (2016). While the architecture and evolution of the Picuris orogen remain enigmatic, evidence for the existence and extent of the orogen keeps increasing.

8. Conclusion

We investigated an area in the central Colorado Front Range in order to decipher the regional folding history away from shear zones and overprinting effects of Cenozoic orogenic and extensional events. The oldest rocks were likely deposited in the Paleoproterozoic, while deposition of a quartzite occurred after ~ 1.43 Ga, but before ~ 1.39–1.33 Ga metamorphism, and possibly later than the ~ 1.49–1.43 Ga basins of Arizona and New Mexico. The area was affected by four generations of folding and metamorphism occurred at mid-crustal pressures of ~ 4 kbar and temperatures of 500–700 °C. This is the first evidence for Mesoproterozoic sediment deposition and widespread folding in Colorado. The impact and extent of the Picuris orogeny in the southwestern U.S. may thus be larger than previously interpreted.

CRediT authorship contribution statement

Asha A. Mahatma: Investigation, Writing – original draft, Visualization. **Yvette D. Kuiper:** Funding acquisition, Conceptualization, Investigation, Writing – original draft, Visualization. **Christopher S. Holm-Denoma:** Writing – review & editing.

Declaration of Competing Interest

The authors declare the following financial interests/personal relationships which may be considered as potential competing interests: [Yvette D. Kuiper reports financial support was provided by US Geological Survey].

Data availability

Data are available in the supplementary data files.

Acknowledgements

Support for this project was provided by the U.S Geological Survey, National Cooperative Geologic Mapping Program under STATEMAP agreement G17AC00143 for fiscal year 2017. Matt Morgan and Scott Fitzgerald from the Colorado Geological Survey, and Cal Ruleman and Scott Minor from the U.S. Geological Survey helped with mapping and digitization. Mike Doe provided construstive comments on an earlier version of this manuscript. Katharina Pfaff provided help with AM and FE-SEM. Journal reviewers Brendan Murphy and two anonymous reviewers, and U.S. Geological Survey internal reviewer Jamey Jones helped us improve the scientific interpretations and the presentation. Any use of trade, firm, or product names is for descriptive purposes only and does not imply endorsement by the U.S. Government.

Data availability

Supplementary data are available with this manuscript.

Appendix A. Supplementary material

Supplementary data to this article can be found online at https://doi.org/10.1016/j.precamres.2022.106878.

References

Aleinikoff, J.N., Reed, J.C., Wooden, J.L., 1993. Lead isotopic evidence for the origin of Paleo-and Mesoproterozoic rocks of the Colorado Province, USA. Precambr. Res. 63 (1-2), 97–122.

Aleinikoff, J.N., Schenck, W.S., Plank, M.O., Srogi, L., Fanning, C.M., Kamo, S.L., Bosbyshell, H., 2006. Deciphering igneous and metamorphic events in high-grade rocks of the Wilmington Complex, Delaware: Morphology, cathodoluminescence and backscattered electron zoning, and SHRIMP U-Pb geochronology of zircon and monazite. Geol. Soc. Am. Bull. 118 (1-2), 39–64.

Allen, J.L., Shaw, C.A., 2011. Seismogenic structure of a crystalline thrust fault: fabric anisotropy and coeval pseudotachylyte-mylonitic pseudotachylyte in the Grizzly Creek Shear Zone, Colorado. Geol. Soc. Lond., Special Publication 359 (1), 135–151.

Anderson, J.L., 1983. Proterozoic anorogenic granite plutonism of North America. Geol. Soc. Am. Mem. 161, 133–154.

Anderson, J.L., Cullers, R.L., 1999. Paleo- and Mesoproterozoic granite plutonism of Colorado and Wyoming. Rocky Mt Geol. 34, 149–164.

Aronoff, R., 2016. The role of the Picuris Orogeny in the Tectonic Evolution of Proterozoic North America. West Lafayette, Indiana, Purdue University, p. 178 p. [Ph.D. thesis].

Aronoff, R.F., Andronicos, C.L., Vervoort, J.D., Hunter, R.A., 2016. Redefining the metamorphic history of the oldest rocks in the southern Rocky Mountains. Geol. Soc. Am. Bull. 128, 1207–1227.

Bennett, V.C., DePaolo, D.J., 1987. Proterozoic crustal history of the western United States as determined by neodymium isotopic mapping. Geol. Soc. Am. Bull. 99, 674–685.

Bickford, M.E., Van Schmus, W.R., Zietz, I., 1986. Proterozoic history of the midcontinent region of North America. Geology 14, 492–496.

Bickford M.E., Cullers R.L., Shuster R.D., Premo W.R., Van Schmus W.R., 1989. U–Pb zircon geochronology of Proterozoic and Cambrian plutons in the Wet Mountains and southern Front Range, Colorado. In: Grambling J.A. Tewksbury B.J., eds., Proterozoic Geology of the Southern Rocky Mountains. Geological Society of America Special Paper 235, 49–64.

Bickford, M.E., Van Schmus, W.R., Karlstrom, K.E., Mueller, P.A., Kamenov, G.D., 2015. Mesoproterozoic-trans-Laurentian magmatism: A synthesis of continent-wide age distributions, new SIMS U-Pb ages, zircon saturation temperatures, and Hf and Nd isotopic compositions. Precambr. Res. 265, 286–312.

Black, L.P., Kamo, S.L., Allen, C.M., Davis, D.W., Aleinikoff, J.N., Valley, J.W., Mundil, R., Campbell, I.H., Korsch, R.J., Williams, I.S., Foudoulis, C., 2004. Improved $^{206}Pb/^{238}U$ microprobe geochronology by the monitoring of a trace-element-related matrix effect; SHRIMP, ID–TIMS, ELA–ICP–MS and oxygen isotope documentation for a series of zircon standards. Chemical Geology 205, 115–140. https://doi.org/10.1016/j.chemgeo.2004.01.003.

Bowring, S.A., Karlstrom, K.E., 1990. Growth, stabilization, and reactivation of Proterozoic lithosphere in the southwestern United States. Geology 18, 1203–1206.

Bryant, B., McGrew, L.W., Wobus, R.A., 1981. Geologic map of the Denver 1° × 2° quadrangle, north-central Colorado: U.S. Geological Survey Miscellaneous Investigations Series Map 1-1163, scale 1:250,000.

Caine, J.S., Minor, S.A., 2009. Structural and geochemical characteristics of faulted sediments and inferences on the role of water in deformation, Rio Grande Rift, New Mexico. Geol. Soc. Am. Bull. 121 (9-10), 1325–1340.

Caine, J.S., Ridley, J., Wessel, Z.R., 2010. To reactivate or not to reactivate – nature and varied behavior of structural inheritance in the Proterozoic basement of the eastern Colorado Mineral Belt over 1.7 billion years of earth history. in Morgan, L.A., and

Quane, S.L., eds., Through the Generations: Geologic and Anthropogenic Field Excursions in the Rocky Mountains from Modern to Ancient. Geological Society of America Field Guide 18, 119–140.

Chapin, C.E., 2012. Origin of the Colorado Mineral Belt. Geosphere 8 (1), 28–43.

Chapin, C.E., Cather, S.M., 1994. Tectonic setting of the axial basins of the northern and central Rio Grande rift. Geol. Soc. Am. Spec. Pap. 291, 5–25.

Condie, K.C., 1982. Plate-tectonics model for Proterozoic continental accretion in the southwestern United States. Geology 10, 37–42.

Condie, K.C., 1986. Geochemistry and tectonic setting of early Proterozoic supracrustal rocks in the southwestern United States. J. Geol. 94 (6), 845–864.

Conway, C.M., Silver, L.T., 1989. Early Proterozoic rocks (1710–1615 Ma) in central to southeastern Arizona. Arizona Geol. Soc. Digest 17, 165–186.

Corfu, F., Hanchar, J.M., Hoskin, P.W.O., Kinny, P., 2003. Atlas of zircon textures. Rev. Mineral. Geochem. 53, 469–500.

Cullers, R.L., Griffin, T., Bickford, M.E., Anderson, J.L., 1992. Origin and chemical evolution of the 1360 Ma San Isabel Batholith, Wet Mountains, Colorado: A mid-crustal granite of anorogenic affinities. Geol. Soc. Am. Bull. 104, 316–328.

Daniel, C.G., Pyle, J.M., 2006. Monazite-xenotime thermochronometry and Al_2SiO_5 reaction textures in the Picuris Range, Northern New Mexico, USA: New evidence for a 1450–1400 Ma orogenic event. J. Petrol. 47, 97–118.

Daniel, C.G., Jones, J.V., III, Andronicos, C.L., Gray, M.B., 2013a. Making the case for the Picuris orogeny: Evidence for a 1500 to 1400 Ma orogenic event in the southwestern United States. In: Abbott, L.D., Hancock, G.S., eds., Classic Concepts and New Directions: Exploring 125 Years of GSA Discoveries in the Rocky Mountain Region. Geological Society of America Field Guide 33, 205–235, doi:10.1130/2013.0033 (07).

Daniel, C.G., Pfeifer, L.S., Jones III, J.V., McFarlane, C.M., 2013b. Detrital zircon evidence for non-Laurentian provenance, Mesoproterozoic (ca. 1490–1450 Ma) deposition and orogenesis in a reconstructed orogenic belt, northern New Mexico, USA: Defining the Picuris orogeny. Geol. Soc. Am. Bull. 125, 1423–1441.

Daniel, C.G., Indares, A., Medaris, L.G., Jr., Aronoff, R., Malone, D., Schwartz, J., 2022. Linking the Pinware, Baraboo, and Picuris orogenies: Recognition of a trans-Laurentian ca. 1520–1350 Ma orogenic belt, in Whitmeyer, S.J., Williams, M.L., Kellett, D.A., and Tikoff, B., eds., Laurentia: Turning Points in the Evolution of a Continent: Geological Society of America Memoir 220, p. 1–16, https://doi.org/10.1130/2022.1220(11).

Daniel, C.G., Pyle, J.M., 2006. Monazite-xenotime thermochronometry and Al2SiO5 reaction textures in the Picuris Range, Northern New Mexico, USA: New evidence for a 1450-1400 Ma orogenic event. Journal of Petrology 47, 97–118. https://doi.org/10.1093/petrology/egi069.

Dann, J.C., 1997. Pseudostratigraphy and origin of the early Proterozoic Payson ophiolite, central Arizona. Geol. Soc. Am. Bull. 109, 347–365.

Doe, M.F., 2014. Reassessment of Paleo- and Mesoproterozoic Basin Sediments of Arizona: Implications for Tectonic Growth of Southern Laurentia and Global Tectonic Configurations. Golden, Colorado School of Mines, p. 676 p. [Ph.D. thesis].

Doe, M.F., Daniel, C.G., 2019. Evidence for Mesoproterozoic ca. 1470–1444 Ma regional deformation of the Mazatzal Group and equivalent rocks in the type area of the Mazatzal orogeny, Tonto Basin, Arizona, in Pearthree, P.A., ed., Geological Excursions in Southwestern North America. Geol. Soc. Am. Field Guide 55, 237–272.

Doe, M.F., Jones III, J.V., Karlstrom, K.E., Dixon, B., Gehrels, G., Pecha, M., 2013. Using detrital zircon ages and Hf isotopes to identify 1.48–1.45 Ga sedimentary basins and fingerprint sources of exotic 1.6–1.5 Ga grains in southwestern Laurentia. Precambr. Res. 231, 409–421.

Doe, M.F., Jones III, J.V., Karlstrom, K.E., Thrane, K., Frei, D., Gehrels, G., Pecha, M., 2012. Basin formation near the end of the 1.60-1.45 Ga tectonic gap in southern Laurentia: Mesoproterozoic Hess Canyon Group of Arizona and implications for ca. 1.5 Ga supercontinent configurations. Lithosphere 4, 77–88.

du Bray, E.A., Holm-Denoma, C.S., Lund, K., Premo, W.R., 2018. Review of the geochemistry and metallogeny of approximately 1.4 Ga granitoid intrusions of the conterminous United States. U.S. Geological Survey no. 2017–5111, 34 p.

English, J.M., Johnston, S.T., Wang, K., 2003. Thermal modelling of the Laramide orogeny: testing the flat-slab subduction hypothesis. Earth Planet. Sci. Lett. 214, 619–632.

Ferguson, C.B., Duebendorfer, E.M., Chamberlain, K.R., 2004. Synkinematic Intrusion of the 1.4-GaBoriana Canyon Pluton, Northwestern Arizona: Implications for Ca. 1.4-Ga Regional Strain in the Westen United States. J. Geol. 112, 165–183.

Frost, C.D., Frost, B.R., 2011. On Ferroan (A-type) Granitoids: their Compositional Variability and Modes of Origin. J. Petrol. 52, 39–53.

Fu, B., Mernagh, T.P., Kita, N.T., Kemp, A.I., Valley, J.W., 2009. Distinguishing magmatic zircon from hydrothermal zircon: a case study from the Gidginbung high-sulphidation Au–Ag–(Cu) deposit, SE Australia. Chem. Geol. 259, 131–142.

Gable, 2000. Geologic map of the Proterozoic rocks of the central Front Range, Colorado. U.S. Geological Survey, IMAP 2605, scale 1:100,000.

Gonzales, D.A., Van Schmus, W.R., 2007. Proterozoic history and crustal evolution in southwestern Colorado: Insight from U/Pb and Sm/Nd data. Precambr. Res. 154, 31–70.

Gonzales, D.A., Karlstrom, K.E., Siek, G.S., 1996. Syncontractional crustal anatexis and deformation during emplacement of ~1435Ma plutons, western Needle Mountains, Colorado. J. Geol. 104, 215–223.

Goodge, J.W., Vervoort, J.D., 2006. Origin of Mesoproterozoic A-type granites in Laurentia: Hf isotope evidence. Earth Planet. Sci. Lett. 243, 711–731.

Goodge, J.W., Vervoort, J.D., Fanning, C.M., Brecke, D.M., Farmer, G.L., Williams, I.S., DePaolo, D.J., 2008. A positive test of East Antarctica-Laurentia juxtaposition within the Rodinia supercontinent. Science 321, 235–240.

Gower, C.F., Krogh, T.E., 2002. A U-Pb geochronological review of the Proterozoic history of the eastern Grenville Province. Can. J. Earth Sci. 39, 795–829.

Grambling, J.A., Codding, D.B., 1982. Stratigraphic and structural relationships of multiply deformed Precambrian metamorphic rocks in the Rio Mora area, New Mexico. Geol. Soc. Am. Bull. 93, 127–137.

Guitreau, M., Mukasa, S.B., Blichert-Toft, J., Fahnestock, M.F., 2016. Pikes Peak batholith (Colorado, USA) revisited: A SIMS and LA-ICP-MS study of zircon U-Pb ages combined with solution Hf isotopic compositions. Precambr. Res. 280, 179–194.

Hedge, C.E., 1969. A petrogenetic and geochronologic study of migmatites and pegmatites in the central Front Range. Golden, Colorado School of Mines, p. 158 p. [Ph.D. thesis].

Holland, M.E., Grambling, T.A., Karlstrom, K.E., Jones, J.V, III, Nagotko, K.N., Daniel, 647 C.G., 2020. Geochronologic and Hf-isotope framework of Proterozoic rocks from central 648 New Mexico, USA: Formation of the Mazatzal crustal province in an extended continental 649 margin arc. Precambrian Research 347, doi:10.1016/j.precamres.2020.105820.

Holm, D.K., Anderson, R., Boerboom, T.J., Cannon, W.F., Chandler, V., Jirsa, M., Miller, J., Schneider, D.A., Schulz, K.J., Van Schmus, W.R., 2007. Reinterpretation of Paleoproterozoic accretionary boundaries of the north-central United States based on a new aeromagnetic-geologic compilation. Precambr. Res. 157, 71–79.

Hu, Z., Gao, S., Liu, Y., Hu, S., Chen, H., Yuan, H., 2008. Signal enhancement in laser ablation ICP-MS by addition of nitrogen in the central channel gas. J. Anal. At. Spectrom. 23, 1093–1101.

Jessup, M.J., Jones III, J.V., Karlstrom, K.E., Williams, M.L., Connelly, J.N., Heizler, M.T., 2006. Three Proterozoic orogenic episodes and an intervening exhumation event in the Black Canyon of the Gunnison region, Colorado. J. Geol. 114, 555–576.

Johannes, W., Holtz, F., 2012. Petrogenesis and Experimental Petrology of Granitic Rocks. Springer-Verlag, Berlin, p. 302 p..

Jones III, J.V., Connelly, J.N., 2006. Proterozoic tectonic evolution of the Sangre de Cristo Mountains, southern Colorado, USA. Rocky Mt Geol. 41, 79–116.

Jones III, J.V., Thrane, K., 2012. Correlating Proterozoic synorogenic metasedimentary successions in southwestern Laurentia: New insights from detrital zircon U-Pb geochronology of Paleoproterozoic quartzite and metaconglomerate in central and northern Colorado, USA. Rocky Mt Geol. 47, 1–35.

Jones III, J.V., Rogers, S.A., Connelly, J.N., 2010a. U-Pb geochronology of Proterozoic granites in the Sawatch Range, central Colorado, U.S.A. Rocky Mt Geol. 45, 1–22.

Jones III, J.V., Siddoway, C.S., Connelly, J.N., 2010b. Characteristics and implications of ca. 1.4 Ga deformation across a Proterozoic mid-crustal section, Wet Mountains, Colorado, USA. Lithosphere 2, 119–135.

Jones III, J.V., Daniel, C.G., Frei, D., Thrane, K., 2011. Revised regional correlations and tectonic implications of Paleoproterozoic and Mesoproterozoic metasedimentary rocks in northern New Mexico, USA: New findings from detrital zircon studies of the Hondo Group, Vadito Group, and Marqueñas Formation. Geosphere 7, 974–991.

Jones III, J.V., Daniel, C.G., Doe, M.F., 2015. Tectonic and sedimentary linkages between the Belt-Purcell basin and southwestern Laurentia during the Mesoproterozoic, ca. 1.60–1.40 Ga. Lithosphere 7, 465–472.

Karlstrom, K.E., Amato, J.M., Williams, M.L., Heizler, M., Shaw, C., Read, A., Bauer, P., 2004. Proterozoic tectonic evolution of the New Mexico region: A synthesis. In: Mack, G.H., and Giles, K.A., eds., The Geology of New Mexico: A Geologic History: Albuquerque, New Mexico. New Mexico Geological Society Special Publication 11, 1–34.

Karlstrom, K.E., Bowring, S.A., 1988. Early Proterozoic assembly of tectonostratigraphic terranes in southwestern North America. J. Geol. 96, 561–576.

Karlstrom, K.E., Humphreys, E.D., 1998. Persistent influence of Proterozoic accretionary boundaries in the tectonic evolution of southwestern North America: Interaction of cratonic grain and mantle modification events. Rocky Mt Geol. 33, 161–179.

Keller, C.B., Schoene, B., 2015. New Constraints From Field Mapping And U-Pb Tims Geochronology On The Magmatic History Of The Needle Mountains Proterozoic Complex, Southwestern Colorado. Geol. Soc. Am. Abstracts Prog. 47, 581.

Kellogg, K.S., Shroba, R.R., Bryant, B., Premo, W.R., 2008. Geologic map of the Denver West 30' x 60' quadrangle, north-central Colorado. In: U.S. Geological Survey Scientific Investigations Map 3000, p. pamphlet..

Kluth, C.F., Coney, P.J., 1981. Plate tectonics of the Ancestral Rocky Mountains. Geology 9, 10–15.

Kopera, J.P., Williams, M.L., Jercinovic, M.J., 2002. Monazite geochronology of the Ortega Quartzite: Documenting the extent of 1.4 Ga tectonism in northern New Mexico and across the orogen. Geol. Soc. Am. Abstracts Prog. 33, No. 4, 10.

Levine, J.S., Mosher, S., Siddoway, C.S., 2013. Relationship between syndeformational partial melting and crustal-scale magmatism and tectonism across the Wet Mountains, central Colorado. Lithosphere 5, 456–476.

Lopez-Sanchez, M.A., Iriondo, A., Marcos, A., Martínez, F.J., 2015. A U-Pb zircon age (479±5 Ma) from the uppermost layers of the Ollo de Sapo Formation near Viveiro (NW Spain): implications for the duration of rifting-related Cambro-Ordovician volcanism in Iberia. Geol. Mag. 152, 341–350.

Ludwig, K.R., 2012. Isoplot 3.75: A geochronological toolkit for Microsoft Excel. Berkley Geochronology Center Special Publication 5.

Lytle, M., 2016. The Proterozoic history of the Idaho Springs-Ralston dhear zone: Evidence for a widespread ca. 1.4 Ga orogenic event in central Colorado [M.Sc. thesis]: Golden, Colorado School of Mines, 89 p.

Mahan, K.H., Allaz, J.A., Baird, G.B., Kelly, N.M., 2013. Proterozoic metamorphism and deformation in the northern Colorado Front Range, in Abbott, L.D., Hancock, G.S., Classic Concepts and New Directions, Exploring 125 Years of GSA Discoveries in the Rocky Mountain Region. Geol. Soc. Am. Field Guide 33, 185–204.

Mahatma, A.A., 2019. The Proterozoic history of the southern half of the Mt. Evans 7.5-minute quadrangle: evidence for a ca. 1.4 Ga orogenic event in the central Front Range, Colorado. M.S. Thesis, Colorado School of Mines, Golden, CO, USA, 88 pp. https://mountainscholar.org/handle/11124/174014.

Mako C.A., 2014. The Timing of Deformation in the Four Peaks Area, central Arizona, and relevance for the Mazatzal Orogeny [M.Sc. thesis]: Amherst, University of Massachusetts-Amherst, 84 p.
Mako, C.A., Williams, M.L., Karlstrom, K.E., Doe, M.F., Powicki, D., Holland, M.E., Gehrels, G., Pecha, M., 2015. Polyphase Proterozoic deformation in the Four Peaks area, central Arizona, and relevance for the Mazatzal orogeny. Geosphere 11, 1975–1995.
McCoy, A.M., 2001. The Proterozoic ancestry of the Colorado Mineral Belt: ca. 1.4 Ga shear zone system in central Colorado [M.Sc. thesis]: Albuquerque, University of New Mexico, 160 p.
McCoy, A.M., Karlstrom, K.E., Shaw, C.A., Williams, M.L., 2005. The Proterozoic ancestry of the Colorado Mineral Belt: 1.4 Ga shear zone system in Central Colorado. In: Karlstrom, K.E., Keller, G.R. (Eds.), The Rocky Mountain Region—An Evolving Lithosphere: Tectonics, Geochemistry, and Geophysics, 154. American Geophysical Union Geophysical Monograph, pp. 71–90.
Medaris, L.G., Singer, B.S., Jicha, B.R., Malone, D.H., Schwartz, J.J., Stewart, E.K., Van Lankvelt, A., Williams, M.L., Reiners, P.W., 2021. Early Mesoproterozoic evolution of midcontinental Laurentia: Defining the geon 14 Baraboo orogeny. Geosci. Front. 12, 101174.
Minor, S.A., Hudson, M.R., Caine, J.S., Thompson, R.A., 2013. Oblique transfer of –extensional strain between basins of the middle Rio Grande rift, New Mexico: fault kinematic and paleostress constraints. Geol. Soc. Am. Spec. Pap. 494, 345–382.
Möller, A., O'Brien, P.J., Kennedy, A., Kröner, A., 2003. Linking growth episodes of zircon and metamorphic textures to zircon chemistry: an example from the ultrahigh- temperature granulites of Rogaland (SW Norway) Geochronology: Linking the Isotopic Record with Petrology and Textures. Geol. Soc. Lond. Spec. Publication 220, 65–81.
Nyman, M.W., Karlstrom, K.E., Kirby, E., Graubard, C.M., 1994. Mesoproterozoic contractional orogeny in western North America: Evidence from ca. 1.4 Ga plutons. Geology 22, 901–904.
Olsen, K.H., Baldridge, W.S., Callender, J.F., 1987. Rio Grande rift: an overview. Tectonophysics 143, 119–139.
Paces, J.B., Miller Jr., J.D., 1993. Precise U-Pb ages of Duluth Complex and related mafic intrusions, northeastern Minnesota: geochonological Insights to physical, petrogenetic, paleomagnetic and tectono-magmatic processes associated with the 1.1 Ga Midcontinentrift system. J. Geophys. Res. 98, 13997–14013.
Paton, C., Hellstrom, J., Paul, B., Woodhead, J., Hergt, J., 2011. Iolite: Freeware for the visualisation and processing of mass spectrometric data. J. Anal. At. Spectrom. 26, 2508–2518.
Premo, W.R., Fanning, C.M., 2000. SHRIMP U-Pb zircon ages for Big Creek gneiss, Wyoming and Boulder Creek batholith, Colorado: Implications for timing of Paleoproterozoic accretion of the northern Colorado province. Rocky Mt Geol. 35, 31–50.
Premo, W.R., Kellogg, K.S., Castineiras, P., Bryant, B., Moscati, R.J., 2007. SHRIMP U-Pb zircon ages and Nd signatures from central Colorado Front Range migmatites and related igneous rocks: Implications for the timing and origin of crustal growth. Geol. Soc. Am. Abst. Prog. 39, A36.
Schaltegger, U., 2007. Hydrothermal zircon. Elements 3, 51–79.
Selverstone, J., Hodgins, M., Aleinikoff, J.N., Fanning, C.M., 2000. Mesoproterozoic reactivation of a Paleoproterozoic transcurrent boundary in the northern Colorado Front Range: Implication for ~1.7- and 1.4-Ga tectonism. Rocky Mountain. Geology 35 (2), 139–162.
Shah, A.A., Bell, T.H., 2012. Ninety million years of orogenesis, 250 million years of quiescence and further orogenesis with no change in PT: Significance for the role of deformation in porphyroblast growth. J. Earth Syst. Sci. 121, 1365–1399.
Shaw, C.A., Allen, J.L., 2007. Field rheology and structural evolution of the Homestake shear zone, Colorado. Rocky Mt Geol. 42, 31–56.
Shaw, C.A., Snee, L.W., Selverstone, J., Reed Jr., J.C., 1999. 40Ar/39Ar thermochronology of Mesoproterozoic metamorphism in the Colorado Front Range. J. Geol. 107, 49–67.
Shaw, C.A., Karlstrom, K.E., Williams, M.L., Jercinovic, M.J., McCoy, A.M., 2001. Electron microprobe monazite dating of ca. 1.71–1.65 Ga and ca. 1.45–1.38 Ga deformation in the Homestake Shear Zone, Colorado: Origin and early evolution of a persistent intracontinental tectonic zone. Geology 29, 739–742.
Powell, L., Mahatma, A.A., Kuiper, Y.D., Ruleman, C., 2022. Geologic map of the Mount Evans Quadrangle, Clear Creek and Park counties, Colorado. Scale 1:24,000. Two sheets.
Shaw, C.A., Karlstrom, K.E., McCoy, A.M., Williams, M.L., Jercinovic, M.J., Dueker, K., 2002. Proterozoic Shear Zones in the Colorado Rocky Mountains: From Continental Assembly to Intracontinental Reactivation. In Lageson, D. (ed.) Science at the Highest Level. Geological Society of America Field Guide 3. 102–117.
Siddoway, C.S., Givot, R.M., Bodle, C.D., Heizler, M.T., 2000. Dynamic versus anorogenic setting for Mesoproterozoic plutonism in the Wet Mountains, Colorado: Does the interpretation depend on level of exposure? Rocky Mt Geol. 35, 91–111.
Siddoway, C.S., Jones, J., Williams, M.L., Andronicos, C.L., Connelly, J., Karlstrom, K.E., 2002. The Mesoproterozoic record in the Wet Mountains, Colorado. Geol. Soc. Am. Abst. Prog. 34 (6), 181.
Sims, P.K., Stein, H.J., 2003. Tectonic evolution of the Proterozoic Colorado province, Southern Rocky Mountains: A summary and appraisal. Rocky Mt Geol. 39, 183–204.
Sláma, J., Košler, J., Condon, D.J., Crowley, J.L., Gerdes, A., Hanchar, J.M., Horstwood, M.S.A., Morris, G.A., Nasdala, L., Norberg, N., Schaltegger, U., Schoene, B., Tubrett, M.N., Whitehouse, M.J., 2008. Plešovice zircon- a new natural reference material for U-Pb and Hf isotopic microanalysis. Chem. Geol. 249, 1–35.
Smith, D.R., Noblett, J., Wobus, R.A., Unruh, D., Chamberlain, K.R., 1999. A review of the Pikes Peak Batholith, Front Range, central Colorado: A "type example" of A-type granitic magmatism. Rocky Mountain Geologist 34, 289–312.
Spear, F., Kohn, M., Cheney, J., 1999. P-T paths from anatectic pelites. Contrib. Mineral. Petrol. 134, 17–32.
Spencer, J.E., Pecha, M.E., Gehrels, G.E., Dickinson, W.R., Domanik, K.J., Quade, J., 2016. Paleoproterozoic orogenesis and quartz-arenite deposition in the Little Chino Valley area, Yavapai tectonic province, central Arizona, USA. Geosphere 12, 1–21.
Skotnicki, S.J., Gruber, D., 2019. Mesoproterozoic rocks of the McDowell Mountains, Arizona—Journey into the magmatic gap, in Pearthree, P.A., ed. Geol. Excursions Southwestern North America: Geol. Soc. Am. Field Guide 55, 169–186. https://doi.org/10.1130/2019.0055(07).
Tucker, R.D., Gower, C.F., 1994. A U-Pb geochronological framework for the Pinware terrane, Grenville Province, southeast Labrador. J. Geol. 102, 67–78.
Tweto, O., 1987. Rock units of the Precambrian basement in Colorado. U.S. Geological Survey Professional Paper 1321-A, A1–A54.
Tweto, O., Sims, P.K., 1963. Precambrian Ancestry of the Colorado Mineral Belt. Geol. Soc. Am. Bull. 74, 991–1014.
Whitmeyer, S.J., Karlstrom, K.E., 2007. Tectonic model for the Proterozoic growth of North America. Geosphere 3, 220–259.
Widmann, B.L., Kirkham, R.M., Beach, S.T., 2000. Geologic map of the Idaho Springs quadrangle, Clear Creek County, Colorado. Colorado Geological Survey Open File Report-00-2SR, scale 1:24,000.
Wilson, E.D., 1939. Pre-Cambrian Mazatzal revolution in central Arizona. Geol. Soc. Am. Bull. 50, 1113–1163.
Windley, B.F., 1993. Proterozoic anorogenic magmatism and its orogenic connections, Fermor Lecture 1991. J. Geol. Soc. 150, 39–50.
Wooden, J.L., DeWitt, E., 1991. Pb isotopic evidence for the boundary between the early Proterozoic Mojave and central Arizona crustal provinces in western Arizona, *in* Karl- strom, K.E., ed. Proterozoic Geology and Ore Deposits of Arizona. Arizona Geol. Soc. Digest 19, 27–50.
Wooden, J.L., Stacey, J.S., Howard, K.A., Doe, B.R., Miller, D.M., 1988. Pb isotopic evidence for the formation of Proterozoic crust in the southwestern United States, *in* Ernst, W.G., ed., Metamorphism and Crustal Evolution of the Western United States, Rubey Volume, Englewood Cliffs, New Jersey, Prentice-Hall 7, 68–86.
Yakymchuk, C., Kirkland, C.L., Clark, C., 2018. Th/U ratios in metamorphic zircon. J. Metamorph. Geol. 36, 715–737.
Ye, H., Royden, L., Burchfield, C., Schuepbach, M., 1996. Late Paleozoic Deformation of Interior North America: The Greater Ancestral Rocky Mountains. Am. Assoc. Pet. Geol. Bull. 80, 1397–1432.